

Politecnico di Torino

Politecnico di Torino

Master's Degree in Environmental and Land Engineering

Industrial Environmental Sustainability

A.y. 2025/2026

Master's Degree Thesis

Evaluation of commercial membranes for the selective separation of lithium and magnesium in aqueous brines

Supervisor:

Prof. Alberto Tiraferri

Candidate:

Claudia Candiotto

September 2026

Abstract

The growing demand for lithium, driven by the development of electric mobility and energy storage systems, has made it necessary to develop more efficient and sustainable extraction technologies. Among these, Direct Lithium Extraction (DLE) from brines using membranes represents a promising solution, but the selective separation of lithium from magnesium remains one of the main challenges. The objective of this thesis was therefore to evaluate the performance of two commercial nanofiltration membranes, TS50 and XPNF, in the selective separation of these ions.

The study involved a literature review on lithium, extraction technologies, and nanofiltration mechanisms, followed by an experimental campaign using flat-sheet membranes. The membranes were characterized through hydraulic tests and evaluated in lithium-magnesium separation tests, both under standard conditions and at different salinity levels.

The experimental results allowed to compare the performance of the two membranes in terms of permeance, selectivity, and separation efficiency, highlighting the influence of membrane characteristics and solution composition. Of the two membranes examined, the TS50 showed the most promising performance, confirming the potential of nanofiltration as a technology for DLE processes.

Index

Abstract i
Index iii
1. Introduction 1
2. Lithium 3
2.1 Global availability 4
2.2 Lithium resources 8
2.2.1 Lithium in igneous rocks 8
2.2.2 Lithium in clays 8
2.2.3 Lithium in brines 9
2.2.4 Lithium in batteries 9
2.3 Direct lithium extraction (DLE) from brines 10
3. Membranes 11
3.1 Definition and function 11
3.2 Filtration types 12
3.3 Materials 13
3.4 Geometries 14
3.5 Structures 15
3.6 Pressure-driven separation processes 16
3.7 Membranes used for laboratory tests 18
4. Nanofiltration and ionic separation of lithium and magnesium 21
4.1 Separation mechanisms 22
4.2 Size sieving 23
4.3 Donnan effect 23
4.4 Dielectric exclusion 25
4.5 Synergistic interaction between separation mechanisms 25
5. Experimental study 27
5.1 Screening tests on flat-sheet membranes 27
5.1.1 System and equipment 27
5.1.2 Test 1: standard two-step filtration test 36
5.1.3 Test 2: standard lithium–magnesium separation test 40

5.1.4 Test 3: lithium–magnesium separation tests at variable NaCl concentrations 44
5.2 Samples and labels 47
6. Data and results 51
6.1 Test 1: standard two-step filtration test 51
6.1.1 Collected data 51
6.1.2 Results interpretation 56
6.2 Test 2: standard lithium–magnesium separation test 57
6.2.1 Collected data 57
6.2.2 Results interpretation 60
6.3 Test 3: lithium–magnesium separation tests at variable NaCl concentrations. 64
6.3.1 Collected data 64
6.3.2 Results interpretation 73
7. Conclusion 81
7.1 Future developments 82
References 83

1. Introduction

The electrification of transportation and the growing adoption of energy storage systems powered by renewable sources have led, in recent years, to a significant increase in global demand for lithium, making it one of the strategic raw materials for the energy transition. This growth has highlighted the need to develop increasingly efficient and sustainable extraction technologies capable of supporting or replacing conventional processes, which are often characterized by high water consumption, long production times, and significant environmental impacts.

Among the most promising technologies there is the Direct Lithium Extraction (DLE), which allows lithium to be recovered directly from brines using processes that differ from traditional methods. However, one of the main challenges posed by these matrices is the presence of high concentrations of other dissolved ions, particularly magnesium. The selective separation of lithium from magnesium is, in fact, one of the most significant challenges, since the two elements have very similar chemical and physical properties, which makes their separation difficult.

In this context, nanofiltration is a particularly promising solution due to its ability to selectively separate monovalent and divalent ions through a combination of steric and electrostatic phenomena, while operating with low energy consumption and minimal use of chemical reagents. However, the performance of this process depends both on the intrinsic characteristics of the membrane used and on the operating conditions employed.

The objective of this thesis was to evaluate the performance of two commercial nanofiltration membranes, TS50 and XPNF, provided by the MANN+HUMMEL company, in the selective separation of lithium and magnesium ions, with the aim of identifying the most promising membrane for potential use in Direct Lithium Extraction processes. To this end, the strategic role of lithium was first examined, analysing its growing importance in the global energy scenario, the main available resources, and the technologies currently used for its recovery. Subsequently, the fundamental principles of membrane technology were introduced, with particular attention to nanofiltration processes and the mechanisms governing the separation of lithium and magnesium ions.

Based on this theoretical knowledge, an experimental study was developed and conducted at the CWC laboratory at the Politecnico di Torino, with the aim of comparing the performance of the two membranes through a series of laboratory tests.

Specifically, the membranes were characterized, lithium–magnesium separation tests were performed under standard conditions to evaluate the separation of lithium and magnesium ions and lithium–magnesium separation tests were conducted with increasing concentrations of sodium chloride to assess the influence of solution composition on separation performance. The results obtained were then analysed and discussed, allowing for a comparison of the behaviour of the two membranes and the identification of the best solution for future applications in the field of Direct Lithium Extraction.

2. Lithium

Lithium (Li), the third element in the periodic table, is a soft, silvery-white alkali metal that is the twenty-fifth most abundant element in the Earth's crust [1], [2].

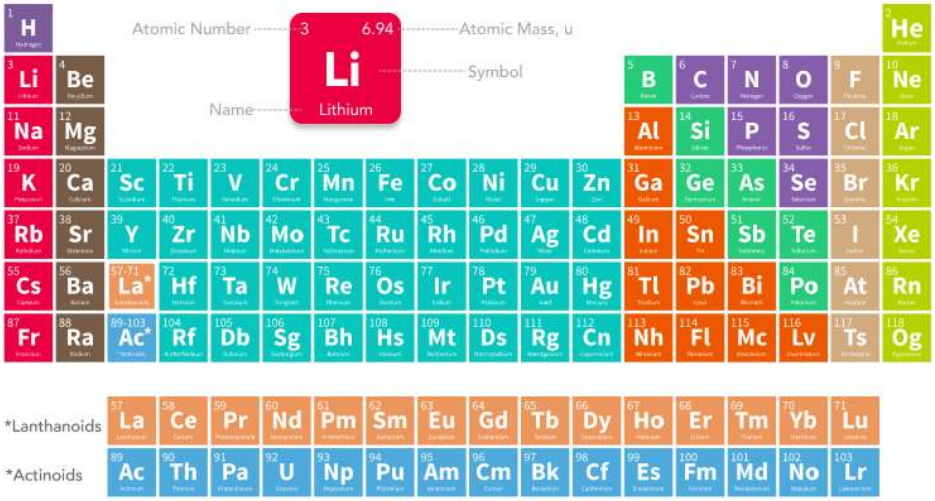


Figure 1. Periodic table [3].

It is considered a strategic resource and one of the most important critical metals for the global energy transition [4]. Its peculiar physical and chemical properties, including low density (0.53 g/cm^3), low atomic weight (6.939), high electrochemical potential, high heat capacity and the lowest electrochemical equivalent among metallic elements (0.259 g/Ah), make it particularly suitable for various technological applications [1], [4].

Thanks to these characteristics, lithium represents the reference material to produce high-performance batteries, capable of providing high voltage, high energy density and storage capacity superior to those obtainable with other metals [1]. Consequently, its use has grown rapidly in recent decades, particularly in the field of rechargeable batteries for portable electronic devices and electric vehicles [2], [4].

In addition to the energy sector, lithium finds application in many other industrial sectors, including for example the production of ceramics, lubricants, pharmaceuticals and even in advanced technologies related to nuclear fusion research [4].

The growing global demand for lithium, mainly driven by the spread of electrochemical storage systems and electric mobility, has however highlighted important critical issues associated with its extraction and processing. Although available resources are considerable, production processes can lead to significant environmental impacts and are influenced by geopolitical factors, market dynamics and supply chain vulnerabilities. For this reason, it is becoming increasingly important

to diversify supply sources and develop more sustainable production technologies and practices in order to ensure security of supply and reduce the environmental impacts associated with the growing demand for this strategic metal [4].

2.1 Global availability

In the context of lithium availability, it is important to distinguish between resources and reserves. Resources represent identified geological stocks that could be exploited through future technological improvements, while reserves correspond to the amount of lithium that is economically extractable under current technological and socioeconomic conditions and thus form the basis of current global lithium production [1], [5].

According to the February 2026 U.S. Mineral Commodity Summary published by the USGS [5], globally available reserves in 2025 totalled 36,470,000 tons, located mainly in the United States, Argentina, Australia, Brazil, Canada, Chile, China, Mali, Portugal, and Zimbabwe.

In contrast, available resources totalled 147,591,000 tons, broken down as follows: Argentina 28 million tons, Bolivia 23 million tons, Chile 13 million tons, Australia 10 million tons, China 10 million tons, Germany 8.9 million tons, Canada 8.1 million tons, Congo 3 million tons, Mexico 1.7 million tons [5].

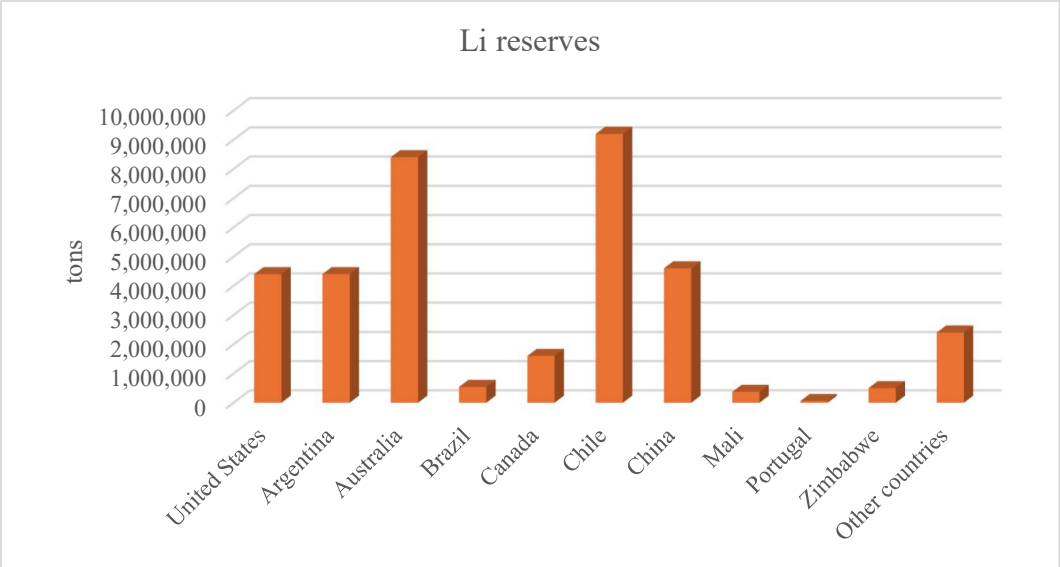


Figure 2. Countries with the largest lithium reserves in 2025. Graph based on data from [5].

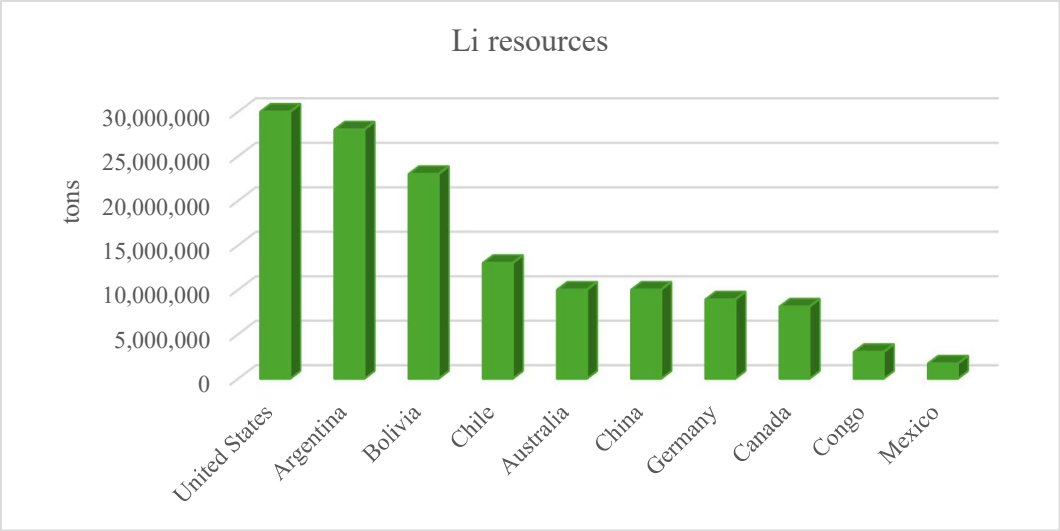


Figure 3. Countries with the largest lithium resources in 2025. Graph based on data from [5].

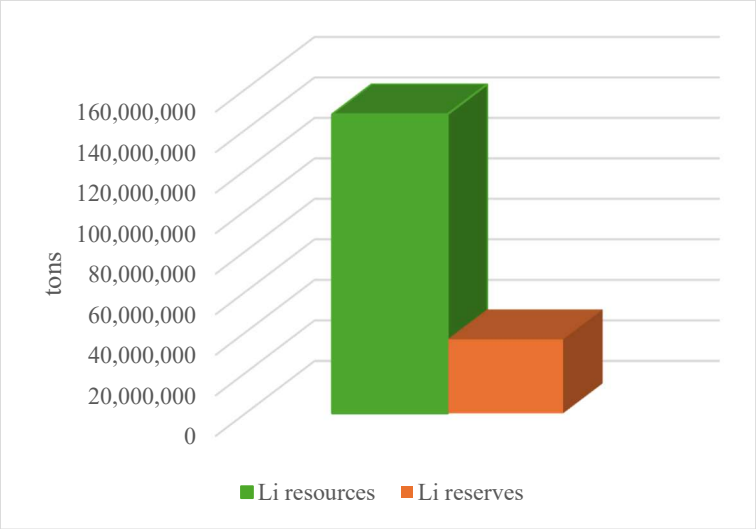


Figure 4. Difference between the total amount of lithium reserves and resources in 2025. Graph based on data from [5].

Global demand for lithium has grown rapidly in recent years, mainly due to the expansion of the electric vehicle market and the increasing use of portable electronic devices [1], [4]. The transition to low-carbon energy systems and policies aimed at reducing greenhouse gas emissions have further increased the demand for this element, which is essential for both electric vehicle batteries and energy storage systems associated with renewable sources, such as solar and wind [1], [2], [4].

In response to this growing demand, global lithium production reached approximately 290,000 tons in 2025, a 31% increase from the 222,000 tons recorded in 2024. During the same period, global consumption increased from approximately 220,000 to 263,000 tons, marking a 20% growth [5].

Furthermore, analysing the data provided by the U.S. Mineral Commodity Summaries from 2015 to the present, it was possible to observe the increasing trend in both production and consumption.

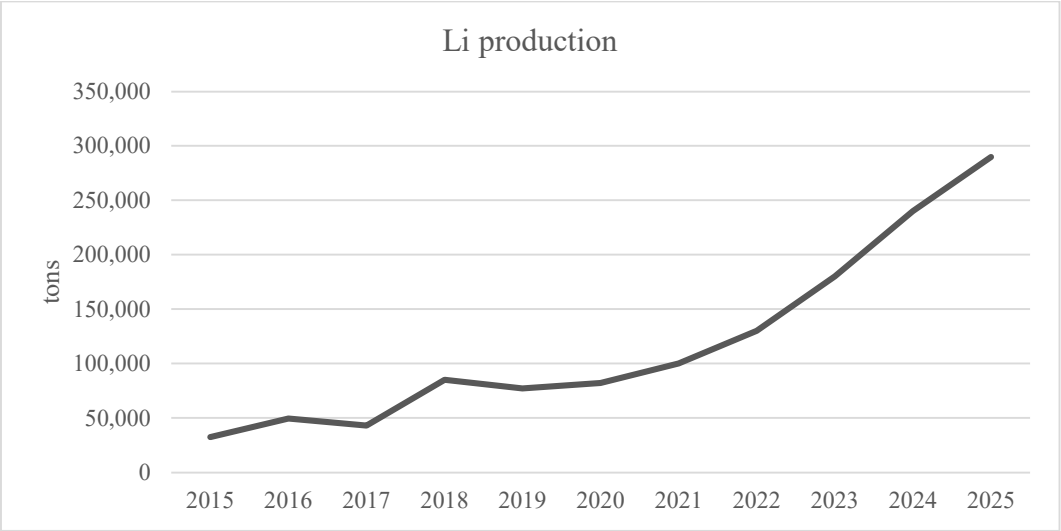


Figure 5. Global lithium production trend from 2015 to 2025. Graph based on data from [5], [6], [7], [8], [9], [10], [11], [12], [13], [14], [15].

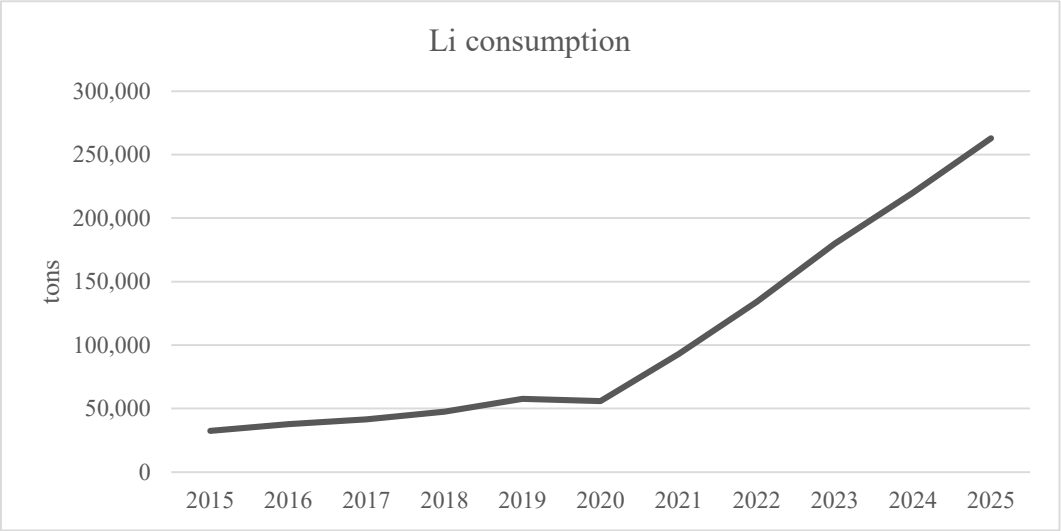


Figure 6. Global lithium consumption trend from 2015 to 2025. Graph based on data from [5], [6], [7], [8], [9], [10], [11], [12], [13], [14], [15].

In addition, globally, in 2025, the primary use of lithium was in the battery sector, which accounted for approximately 88% of total consumption. Other uses include the production of ceramics and glass (4%), lubricating greases (2%), air treatment (1%), flux powders for continuous casting molds (1%), medical applications (1%), and other uses (3%). The predominant share allocated to batteries reflects the growing adoption

of electric vehicles, energy storage systems, portable electronic devices and electrical tools [5].

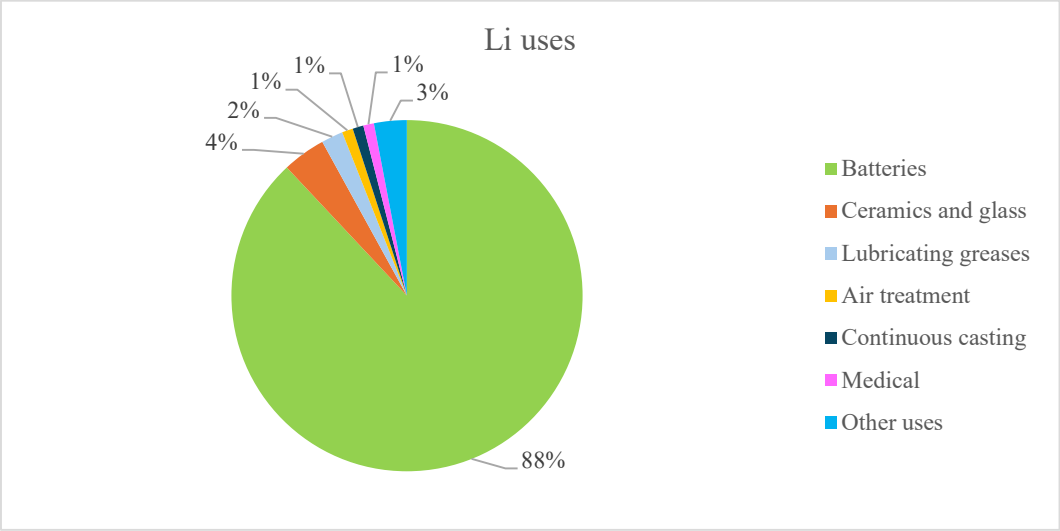


Figure 7. Global lithium use in 2025. Graph based on data from [5].

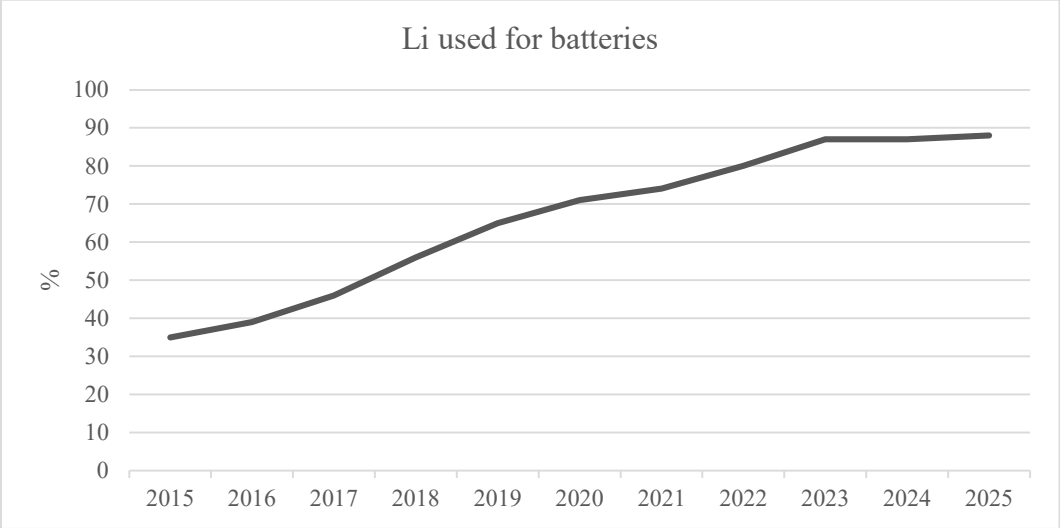


Figure 8. Trend of the amount of lithium, as a percentage, used to produce batteries from 2015 to 2025. Graph based on data from [5], [6], [7], [8], [9], [10], [11], [12], [13], [14], [15].

Despite the abundant availability of resources, some studies highlight the risk that currently known lithium reserves could be depleted by 2080 if consumption continues to grow at the current rate [4].

Furthermore, global lithium production and supply are concentrated in a limited number of countries, increasing geopolitical vulnerabilities and supply chain risks. These factors have increased interest in alternative sources of lithium, recovery

technologies, and recycling strategies capable of ensuring a more sustainable, diversified, and secure supply chain in the long term [2].

2.2 Lithium resources

Lithium is widely distributed in nature; however, in the Earth's crust, it is not generally found in its elemental form, but it can be found in various matrices, including igneous rocks, clay deposits, brines, and seawater [1], [2], [4]. From an economic and production point of view, the main sources of supply are brines and minerals found in igneous rocks, which form the basis of the current lithium extractive industry [1], [4]. Igneous rocks and brines are therefore the most significant resources at global level, contributing respectively to approximately 14% and 78% of known lithium resources. Furthermore, from a production point of view, these two types of deposits provide almost all the extracted lithium, contributing respectively to approximately 25% and 65% of global production [4].

Currently, salt lake brines are the main source of commercial lithium production due to their widespread availability and generally lower extraction costs compared to hard rock deposits. However, increasing global demand for lithium and environmental concerns associated with conventional extraction methods have stimulated interest in alternative or unconventional sources. These include geothermal brines, seawater, and spent lithium-ion batteries (LIBs). However, despite their high potential, the exploitation of these unconventional sources still presents significant technological and economic challenges [2].

2.2.1 Lithium in igneous rocks

The most significant igneous lithium deposits are found in granitic pegmatites. Within these formations, lithium is present in various mineral species. Among these, spodumene is the mineral of greatest commercial interest for large-scale lithium production, due to its high lithium content [1], [4].

2.2.2 Lithium in clays

Lithium-bearing clays represent the world's third-largest source of lithium and account for approximately 10% of total lithium production. The main lithium-bearing clay minerals include hectorite and jadarite [4].

2.2.3 Lithium in brines

In brines, lithium is present mainly in ionic form as Li^+ and these can be divided into three main categories: continental, geothermal and oilfield [4]. Continental brines, also known as salt lake brines or salars, are the major source of lithium production from brines [4]. These are hypersaline aquifers characterized by high concentrations of dissolved ions, generally located in underground reservoirs within closed basins, where the surrounding rock formations contribute to the release of dissolved elements into the brine [1]. These brines are characterized by lithium concentrations generally between 54 and 1600 mg/L and are found predominantly in salt lakes of Argentina, Bolivia and Chile, an area known as the "lithium triangle" [4]. Lithium extraction from continental brines is considered cheaper than from hard rock ores, with costs 30–50% lower, making it the most preferred source of supply for investors [1].

Furthermore, geothermal and oilfield brines also represent potential sources of lithium. These are derived from geothermal energy production and oil and gas extraction activities, respectively, and have generally lower lithium concentrations, up to about 400 mg/L. Seawater also represents a potential resource, although the lithium concentration is much lower, at about 0.17 mg/L [4].

A key critical aspect of brines containing lithium is the presence of high concentrations of other dissolved ions, including sodium (Na^+), magnesium (Mg^{2+}), calcium (Ca^{2+}), potassium (K^+), strontium (Sr^{2+}), and borate ($B(OH)_4^-$), impurities that can complicate separation processes and reduce the efficiency of lithium recovery [4].

2.2.4 Lithium in batteries

Lithium-ion batteries (LIBs) are electrochemical devices that store and release energy through the movement of lithium ions between anode and cathode [4]. Thanks to the electrochemical properties of lithium, in particular its high reactivity and favourable redox potential, this technology ensures high performance in energy storage systems [2]. LIBs are today considered among the most efficient solutions available, as they combine high mass and volumetric energy density, high coulombic efficiency, high output voltage, low weight and a long lifetime [1]. These characteristics, combined with ease of recharging, good performance at high temperatures and the possibility of recovering and recycling part of the components at the end of their life, have favoured their widespread diffusion in consumer electronics and electric mobility, making them consistent with the principles of the circular economy [1], [4].

LIBs are made up of several components: cathode, anode, electrolyte, separator, current collectors and battery case. The cathode represents the source of lithium ions, while the anode, generally made of graphite, allows their intercalation during the

charging phase. The electrolyte, normally consisting of a lithium salt dissolved in an organic solvent, allows the transfer of ions between the two electrodes, while the porous separator prevents direct contact between the anode and cathode while allowing the passage of ions. The current collectors, typically made of aluminium for the cathode and copper for the anode, facilitate the transfer of electrons, while the casing ensures structural integrity and protects the internal components [1], [4].

Lithium-ion batteries typically contain between 2 and 7% of lithium by weight [4]. For this reason, used batteries represent an important secondary resource for the recovery of this element and a potential more sustainable alternative to conventional sources [4]. The recovery of lithium from secondary resources is considered crucial to meet the growing global demand for this metal and to support the transition towards the electrification of transport [1]. Furthermore, this approach can contribute to the diversification of supply sources and to a less resource-intensive lithium production [1].

2.3 Direct lithium extraction (DLE) from brines

The growing demand for lithium and the environmental, water and energy issues associated with conventional extraction methods, such as brine evaporation and hard rock extraction, have driven the development of alternative technologies for the recovery of this element [2]. In this context, Direct Lithium Extraction has emerged as one of the most promising solutions for lithium recovery from brines [2], [4].

Compared to traditional evaporative processes, DLE offers several advantages, including significantly shorter production times, which can be reduced from months or years to hours or days, higher lithium recovery rates, and lower land and water use. Thus, this technology reduces the environmental impact of the extraction process, can operate independently of climatic conditions, and has the potential for recycling the water used in the process [4].

The sustainability and economic feasibility of DLE processes depend on several factors, including the Li^+ concentration in the brine, the presence of competing ions expressed, for example, by the Li/Mg ratio, the costs of materials and operations, the duration of the production cycle and the lithium market conditions [4].

Numerous approaches for the sustainable recovery of lithium from brines and other alternative resources have been developed and studied [4]. Major DLE technologies include adsorption, ion exchange, solvent extraction, membrane processes, and electrochemical systems [1], [4]. Specifically, ion exchange, selective adsorption, and membrane processes are considered among the most promising to improve extraction efficiency and overcome the limitations of conventional methods [2].

3. Membranes

3.1 Definition and function

A membrane can be defined as a thin, discrete interface that separates two phases and acts as a selectively permeable barrier, regulating the transport of chemical species with which it comes into contact. Its main function is to allow the preferential passage of certain components, limiting or preventing that of others, making it possible to separate mixtures based on the properties of the different species present [16], [17], [18].

From a structural point of view, membranes can present very different characteristics. In fact, they can be homogeneous or heterogeneous, symmetrical or asymmetrical, solid or liquid, and can be made of organic or inorganic materials. Furthermore, they can be electrically neutral or possess positive or negative charges and specific functional groups, capable of promoting binding or complexation phenomena with particular chemical species [16], [18].
The high variety of materials and configurations makes it difficult to describe a membrane solely based on its structure; for this reason, it is generally identified above all on the basis of the role it plays in the separation process. The common feature of all materials used as membranes is in fact the ability to limit the passage of different species in a highly selective manner [16].

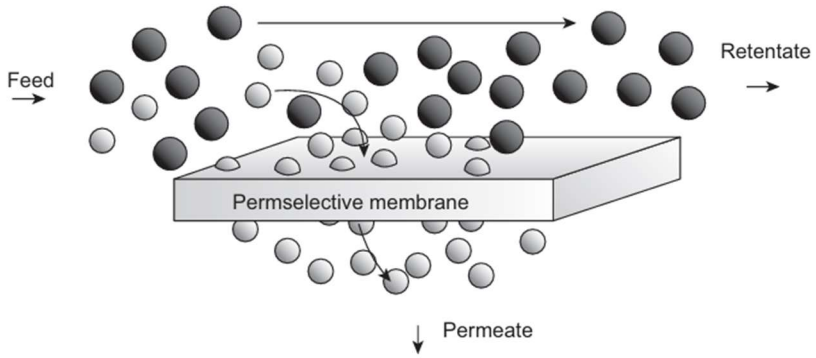


Figure 9. Membrane system [17].

The separation achieved by a membrane process results from the different transport rates of the mixture's components across the membrane itself. This transport is governed by both the intrinsic properties of the membrane, such as the concentration and mobility of the species in its matrix, and the action of appropriate driving forces. These include the pressure gradient, the concentration gradient, the partial vapor pressure gradient, the temperature gradient, and the electric potential gradient, the

presence of which determines the movement of species from one side of the membrane to the other [16], [17]. Furthermore, permeation depends on the intensity of these applied driving forces [17].

The performance of a membrane is generally evaluated through two fundamental parameters: flux and selectivity. Flux represents the quantity of substance, expressed in terms of volume, mass or moles, that passes through the membrane per unit of surface area and time. In the case of volumetric flux, the commonly used unit of measurement is the litre per square meter per hour (L m^{-2} h^{-1} i.e. LMH) [17].
Furthermore, permeance (LMH/bar) measures the ease with which a fluid or dissolved substance can pass through a membrane. It therefore depends on the flow rate and represents the ratio between the flow of the substance and the driving force that determines its passage.
While selectivity describes the membrane's ability to discriminate between the different components of the mixture and is generally expressed through the retention or separation factor [17].

3.2 Filtration types

Membrane separation processes can be conducted mainly according to two different operating configurations: dead-end filtration and cross-flow filtration. The distinction between these operating modes depends on the direction of the feed flow with respect to the membrane surface [17].
In dead-end filtration, both the feed stream and the permeate are directed perpendicular to the membrane surface. In this configuration, the entire feed stream is forced to pass through the membrane, resulting in the accumulation of retained solids on its surface. Due to its simplicity of operation, this mode is widely used in laboratory applications and small-scale separations [17].

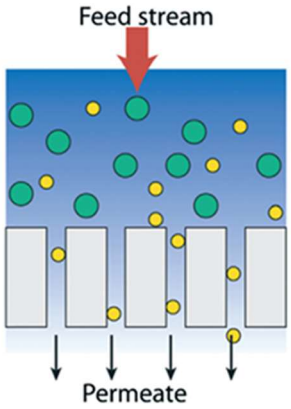


Figure 10. Dead-end filtration scheme [17].

In cross-flow filtration, however, the feed fluid flows parallel to the membrane surface, while only a portion of the flow passes through the membrane, giving rise to the permeate. The tangential motion of the fluid helps to limit the accumulation of material on the membrane surface, making this configuration particularly suitable for continuous processes and industrial-scale applications [17].
This last configuration represents the setup used for laboratory activities in the system described in the following chapters. The cell used will have an inlet feed at the back of the cell, which, flowing over the membrane, will allow the permeate to pass through, while the remaining portion will exit through the retentate tube, also positioned at the back.

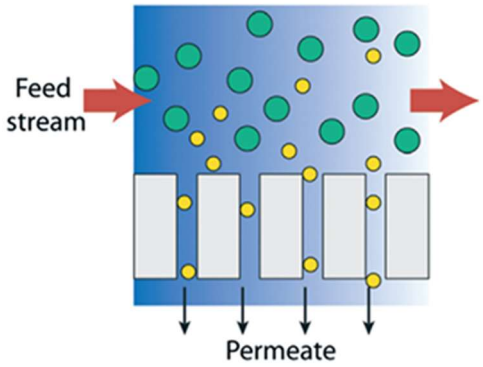


Figure 11. Cross-flow filtration scheme [17].

3.3 Materials

Membranes can be made using a wide variety of materials, including polymers, ceramics, glass, metals, and, in some cases, liquids. Depending on their composition, they can be electrically neutral or have surface charges, characteristics that influence the transport mechanism and the selectivity towards different chemical species [16].

Among the various materials available, polymers represent the most widely used category in the production of membranes thanks to their low cost, high availability and relative simplicity of the manufacturing processes [17].
Among the most widely used polymers, polyamide (PA) and cellulose acetate (CA) are particularly used, especially in the production of membranes intended for nanofiltration (NF) and reverse osmosis (RO) processes. In particular, polyamide is a synthetic polymer characterized by the presence of amide groups (-NHCO-) in the main chain and it is commonly used as a thin and dense active layer in thin-film composite (TFC) membranes, thanks to its high performance in terms of selectivity [17], [18].

3.4 Geometries

The membranes used in separation processes can be made according to different geometries, which influence the design of the filtration module and the application field of the process. The main configurations are flat sheet, tubular, capillary and hollow fibers. Each of them has specific construction and operational characteristics, which determine their suitability for different applications [17].

Flat-sheet membranes represent the simplest configuration and can be assembled typically in plate-and-frame or spiral-wound modules. In plate-and-frame modules, one or more flat membranes are inserted between rigid supports that delimit the feed flow channel. This configuration is widely used in laboratory applications thanks to its simple construction, the ease of membrane replacement and the possibility of operating in well-controlled experimental conditions [17]. In fact, the membranes used in this work belong to the flat sheet typology with plate-and-frame module.



Figure 12. Flat sheet membranes in the plate-and-frame configuration used for laboratory tests.

In the spiral-wound module, on the other hand, the flat membranes are separated by flexible supports and spirally wrapped around a central porous tube intended for collecting the permeate. This configuration allows for a high filtration surface area in a small volume and it is therefore one of the most widespread in industrial nanofiltration and reverse osmosis applications [17].

Membranes with a circular cross-section include tubular, capillary and hollow fiber configurations, which are mainly distinguished by their internal diameter. Tubular membranes have the largest diameter, capillary membranes have intermediate dimensions, while hollow fibers are characterised by the smallest diameters, allowing a very high filtering surface to be concentrated in modules of small dimensions [17].

3.5 Structures

Synthetic membranes can have very different physical structures, which directly influence their behaviour in separation processes. Based on their morphology and transport mechanism, they can be classified into four main categories: porous membranes, dense (or homogeneous solid) membranes, electrically charged membranes, and liquid or solid membranes containing selective carriers [16].

From a structural point of view, membranes can also be divided into symmetric (or isotropic) and asymmetric (or anisotropic).

In symmetric membranes, the structure and transport properties remain constant along the entire thickness of the membrane; consequently, permeation is influenced by the entire thickness of the material. Symmetric membranes can be microporous, dense, or electrically charged, depending on the separation mechanism used [16], [17], [18].
Microporous membranes are characterized by a rigid structure containing a network of randomly distributed interconnected pores. In this case, separation occurs mainly through size exclusion: particles larger than the pores are completely rejected, while those of intermediate dimensions can only be partially rejected [18].
Dense membranes, which lack continuous pores, instead achieve separation through a solubility-diffusion mechanism. The permeating species dissolve in the membrane material and diffuse through it under the action of a driving force, such as a pressure gradient, concentration or electrical potential. The separation efficiency therefore depends on the different diffusivities and solubilities of the components within the polymer matrix, allowing even molecules of very similar dimensions to be separated [18].
Electrically charged membranes can be either dense or microporous and can have positively or negatively charged functional groups. In this case, separation is mainly governed by electrostatic exclusion which hinders the passage of ions having the same charge as the functional groups present in the membrane, while the effect of pore size is generally secondary [18].

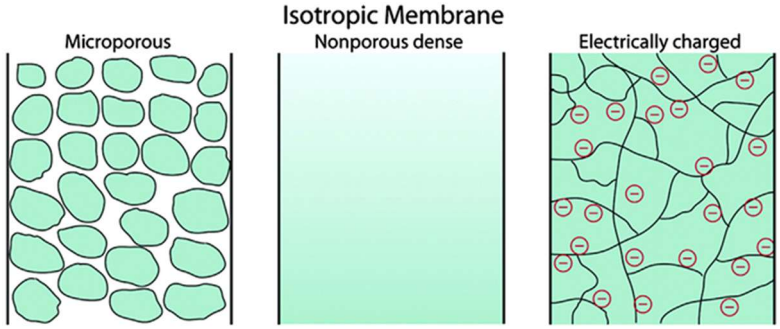


Figure 13. Types of isotropic membranes [17].

Asymmetric (or anisotropic) membranes are currently the most common configuration in membrane separation applications. They consist of a thin, selective surface layer, generally 0.1-1 μm thick, supported by a highly porous substructure approximately 100-200 μm thick, which primarily serves as mechanical support. The surface layer constitutes the effective selective barrier and determines both the separation performance and the permeation rate, while the porous support contributes mainly to the mechanical resistance of the membrane without significantly influencing its transport properties. Since the permeate flux is inversely proportional to the thickness of the selective layer, the realization of membranes with increasingly thinner skins represents a major objective in the development of new materials [16], [17], [18].
Asymmetric membranes can be obtained through two different manufacturing strategies. In the first case, through the phase inversion process, integral asymmetric membranes are created, in which the selective layer and the porous support are made of the same material and are formed in a single production step. In the second case, the so-called composite membranes are obtained, in which the selective layer is deposited on a preformed porous support; in this configuration the two layers are generally made of different materials, allowing to combine high separation performance with adequate mechanical resistance [16], [18].

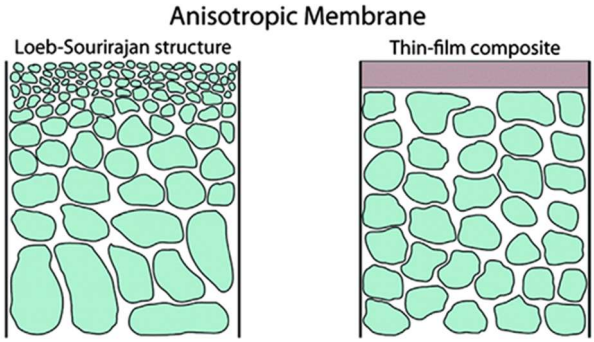


Figure 14. Types of anisotropic membranes [17].

3.6 Pressure-driven separation processes

Among the various membrane separation processes, pressure-driven ones are the most widespread for the treatment of aqueous solutions. In these processes, transmembrane pressure (TMP) represents the driving force that allows the selective transfer of the solvent and some solutes across the membrane, exploiting the different permeabilities of the components of the mixture. The process generates two currents: the permeate, consisting of the species that cross the membrane, and the retentate, containing the rejected species [19].

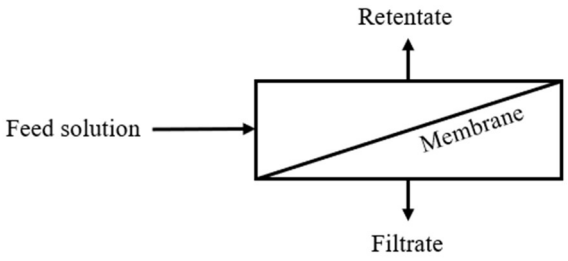


Figure 15. Membrane system scheme.

Pressure-driven membrane processes are commonly classified into microfiltration (MF), ultrafiltration (UF), nanofiltration (NF), and reverse osmosis (RO). Although all require the application of transmembrane pressure, they differ in pore size, operating pressure, and the type of species retained. In general, when moving from microfiltration to reverse osmosis, the pore size decreases and the pressure required to achieve separation increases [17].

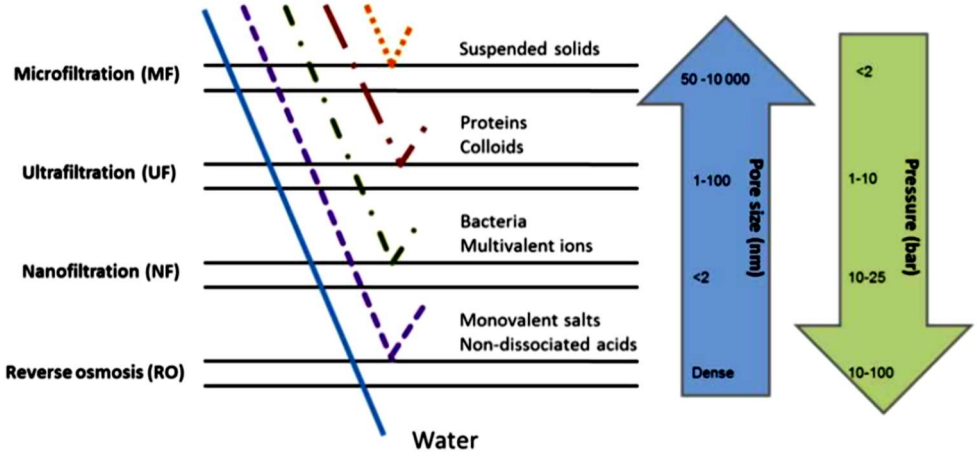


Figure 16. Pressure-driven separation processes: rejected elements, pore size (nm) and pressure (bar) [20].

Microfiltration (MF) is mainly used for the removal of suspended particles and microorganisms, generally with sizes between 10 and 10000 nm, operating at relatively low pressures of approximately 2 bar [17].

Ultrafiltration (UF) instead allows the separation of colloids, macromolecules and biomolecules of smaller dimensions than those retained by microfiltration, having a pore size of approximately 1-100 nm and requiring higher operating pressures of approximately 1-10 bar [17].

Nanofiltration (NF) occupies an intermediate position between ultrafiltration and reverse osmosis, both in terms of operating pressure (10-25 bar) and separation performance (with a pore diameter smaller than 2 nm). NF membranes are generally

able to retain most organic compounds and exhibit significant retention capacity for salts, especially multivalent ones, while allowing the passage of a portion of monovalent salts [17], [18].
Reverse osmosis (RO) represents the membrane process with the highest degree of separation. Operating at higher pressures than other processes (10-100 bar), it allows the removal of almost all dissolved salts and contaminants present in water, reversing the natural osmotic process by applying a pressure higher than the osmotic pressure of the solution [17].

3.7 Membranes used for laboratory tests

This section describes the main characteristics of the membranes used in the laboratory tests, which are explained in the following chapters, with reference to their structure, constituent materials and operational properties.

The membranes used in the experimental tests are the TS50 and XPNF, both produced by MANN+HUMMEL and belonging to the TRISEP commercial line.
These are negatively charged, anisotropic, hydrophilic polymeric membranes for nanofiltration, characterized by different selective layer materials: the TS50 membrane is made of polyamide (PA), while the XPNF membrane is made of polypiperazine (PIPA). According to the manufacturer's technical specifications, both belong to the category of thin-film composite (TFC) membranes, characterized by an asymmetric multilayer structure [21].

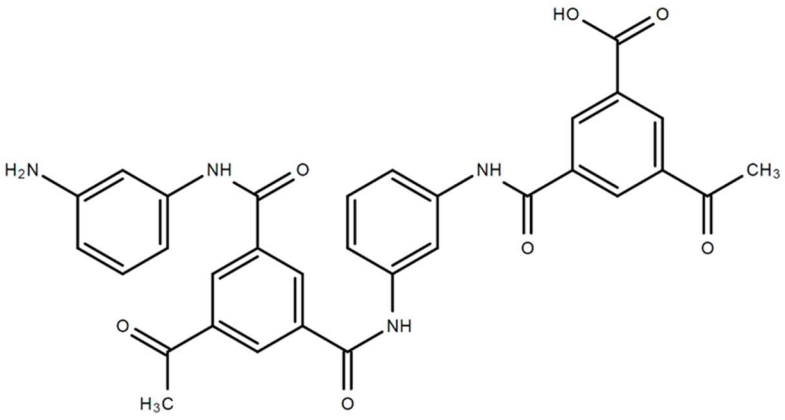


Figure 17. Polyamide membrane structure [21].

Unlike conventional asymmetric membranes, which consist of a selective layer and a single porous support, the TFC membranes used in this study have a structure composed of three functional layers: a thin, dense selective layer of polyamide (or

polypiperazine), a microporous intermediate layer of polysulfone, and a mechanical support layer typically consisting of a polyester nonwoven fabric [21].
The selective layer is responsible for the separation properties and represents the functional element of the membrane, responsible for the permeation of water and the rejection of salts [21].
The support layer provides strength to the membrane, increasing its overall structural resistance and protecting it from mechanical stress and chemical degradation. It therefore ensures stability during operation even at high pressures. However, since it is too irregular and porous to provide a suitable base for the barrier layer, a microporous polysulfone substrate act as an intermediate layer [21].
The intermediate polysulfone layer allows for uniform distribution of mechanical stresses and provides support to the active layer without hindering mass transport [21].

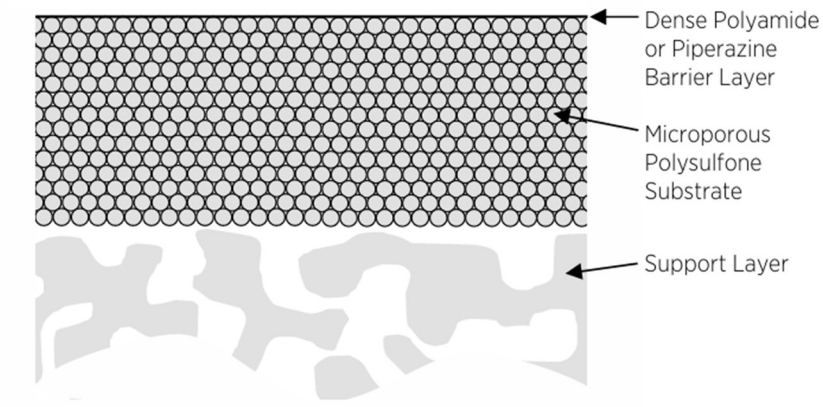


Figure 18. Structure of thin film composite membranes [21].

Thin-film composite membranes also present numerous operational advantages compared to other types of membranes. They can operate in a wide pH range (1-12), withstand temperatures up to 80 °C, allow working at relatively low pressures and show good resistance to hydrolysis, guaranteeing high performance and a long operating life. However, a limitation of this type of membrane is represented by its sensitivity to chlorine, which, after prolonged exposure, can degrade the active layer compromising its separation performance [21].

4. Nanofiltration and ionic separation of lithium and magnesium

Lithium extraction from brines represents one of the main challenges in the recovery of this resource, both due to the great variability of the Li^+ concentration, which can range from a few ppm to several hundred ppm, and due to the presence of numerous coexisting ions, such as Mg^{2+}, Na^+, Ca^{2+}, K^+ and Cl^-. In particular, the high Li/Mg ratio typical of many brines constitutes one of the main obstacles to the selective extraction of lithium, since Li^+ and Mg^{2+} ions exhibit very similar chemical-physical properties with regard to their behaviour in solution. The hydrated ionic radius of Li^+ is in fact equal to approximately 0.38 nm, while that of Mg^{2+} is approximately 0.43 nm, making a separation based exclusively on ion size particularly difficult [22], [23].

Table 1. Summary table of the physical-chemical properties of the main cations present in the synthetic brines used in the experimental tests explained in the following chapters [24].

Ionic species	Ionic radius (nm)	Hydration radius (nm)	Hydration energy (kcal / mol)	Diffusion coefficient (10^{-9} m^2 / s)
Li^+	0.060	0.382	113.5	1.03
Mg^{2+}	0.065	0.428	437.5	0.706
Na^+	0.095	0.358	87.2	1.33

Various technologies have been developed for lithium recovery from brines, including precipitation, adsorption, solvent extraction, electrochemistry, electrodialysis, and membrane separation processes. However, conventional techniques mentioned often have limitations such as long processing times, low lithium recovery rates, the use of large amounts of chemical reagents, suboptimal resource utilization and reduced environmental sustainability. On the contrary, nanofiltration (NF) has established itself as one of the most promising technologies thanks to its operational simplicity, low energy consumption, absence or limited use of chemical reagents, high selectivity towards ions and greater environmental compatibility [22], [23], [25].

Different types of nanofiltration membranes have been developed to increase the efficiency of Li^+/Mg^{2+} separation, which can be classified into negatively charged, positively charged, mixed-charge, size-sieving, and bionic membranes [22], [24].
However, considering that the present experimental work employed negatively charged membranes, with neutral or slightly positive behaviour, the subsequent analysis will focus on these specific categories.

4.1 Separation mechanisms

From the point of view of mass transport, nanofiltration represents an intermediate technology between ultrafiltration and reverse osmosis also with regard to the separation mechanism. While microporous membranes operate mainly by steric exclusion (pore flow) and dense membranes follow the solution-diffusion model, NF membranes combine both mechanisms. Separation depends on both the size of the permeating species and the electrostatic interactions between the ions and the functional groups present on the membrane surface [26].

In the specific case of the separation between Mg^{2+} and Li^{+}, the performance of nanofiltration is governed by the combination of three fundamental mechanisms: size sieving, Donnan effect (charge exclusion) and dielectric exclusion [22], [23], [25].

The separation performance of a membrane can be evaluated by its rejection rate, that is, the percentage of contaminants, salts or solutes that a filter membrane retains compared to the total present in the incoming water, which is defined as:

$$R = \left(1 - \frac{C_p}{C_f}\right) * 100$$

where C_p is the concentration in the permeate, while C_f is the concentration in the feed of the element for which the rejection is to be determined [27], [28].
A negative rejection value means that the element passes through the membrane bringing the concentration in the permeate to a higher value than that in the feed, while the higher the rejection, the greater the retention of the solute.

Furthermore, the separation efficiency is generally evaluated by the Li/Mg separation factor, defined as:

$$SF_{Li,Mg} = \frac{C_{Li,p} / C_{Li,f}}{C_{Mg,p} / C_{Mg,f}}$$

where $C_{Li,p}$ and $C_{Mg,p}$ represent the concentrations of Li^{+} and Mg^{2+} in the permeate, while $C_{Li,f}$ and $C_{Mg,f}$ are the respective concentrations in the feed solution. High values of the separation factor indicate a greater capacity of the membrane to favour the

passage of lithium compared to magnesium, while a value equal to 1 means no selectivity and therefore Li and Mg are not separated [22], [27].

4.2 Size sieving

Steric exclusion is based on the difference between the pore sizes of the membrane and the hydrated ions. Ideally, the pores should have dimensions between the hydrated diameter of Li^+ and that of Mg^{2+}, allowing preferential passage of lithium and retaining magnesium. However, the small difference between the hydrated radii of the two ions (0.38 nm for Li^+ and 0.43 nm for Mg^{2+}) and the broad pore size distribution typical of commercial membranes severely limits the effectiveness of this mechanism when considered in isolation [22], [25].

Furthermore, when passing through the smaller pores, the ions must remove part of their hydration shell. Since Li^+ has a significantly lower hydration energy (113.5 kcal/mol) than Mg^{2+} (437.5 kcal/mol), its partial dehydration requires less energy expenditure, favouring its permeation through the membrane [22], [24].

To increase selectivity, membranes characterized by smaller pores and a more uniform size distribution have been developed in recent years. In these membranes, despite the increase in hydraulic resistance and the decrease in flux, the contribution of steric exclusion is significantly amplified, allowing to obtain high values of the Li/Mg separation factor [22].

4.3 Donnan effect

In nanofiltration membranes, ion separation is influenced not only by the pore size, but also by electrostatic interactions between ions and fixed charges present on the surface and inside the membrane. These charges arise from the dissociation of ionizable functional groups and, under neutral or alkaline pH conditions, generally confer a negative surface charge to membranes [18], [22].
Charges from dissociable functional groups on the membrane surface regulate ion transport through the Donnan effect.

In the general functioning of the Donnan effect, co-ions (ions with the same charge as the membrane) undergo electrostatic repulsion, while counter-ions (ions with opposite charge to the membrane) are attracted by the charges of the membrane and tend to accumulate in the pore area or on the membrane surface, forming a concentration gradient between solution and membrane (i.e. a non-uniform distribution of

concentrations), which makes diffusion unfavourable since the distribution of ions generated by the Donnan effect also creates an electric field that opposes the further entry of ions [22], [25], [29].
Thus, co-ions cannot diffuse easily because they are repelled, while counter-ions cannot enter freely on their own, because the system must maintain electro-neutrality: the rejection of co-ions indirectly also hinders the passage of the corresponding counter-ions, which could pass more easily if "accompanied" by co-ions [22], [25], [29].
Furthermore, the electrostatic repulsion due to the Donnan effect is much stronger for co-ions and counter-ions with higher charges. In fact, a charged NF membrane shows a greater electrostatic interaction strength for divalent ions than for monovalent ions, due to the higher charge number of divalent ions compared to monovalent ones [22].

In the experimental tests conducted in this thesis, negatively charged membranes were used, however, a pH of 3.3 was set in the laboratory tests. Under these conditions, the high concentration of H^+ ions causes the protonation of most of the membrane's surface carboxyl groups, with the conversion of deprotonated carboxyl groups ($-COO^-$) into neutral carboxyl groups (-COOH). Consequently, the membrane's negative charge density is significantly reduced.
Furthermore, polyamide membranes can contain amino groups which, in an acidic environment, tend to protonate according to the reaction: $-NH_2 + H^+ \rightarrow -NH_3^+$.
The protonation of the amino groups, combined with the neutralization of the carboxyl groups, causes the membrane to be near its isoelectric point, that is the condition in which the net surface charge is close to zero. In some cases, the surface may even acquire a weak positive charge. Therefore, under the operating conditions used (pH 3.3), the contribution of electrostatic interactions and thus Donnan exclusion, is significantly reduced compared to what occurs at neutral or alkaline pH, while steric exclusion (paragraph 4.2), ion dehydration(paragraph 4.2) and dielectric exclusion (paragraph 4.4), play a relatively more important role.

In the case of the separation of Li^+ and Mg^{2+}, the contribution of the Donnan effect depends on the surface charge of the membrane. In a negatively charged membrane, both ions are counter-ions and are therefore electrostatically attracted. But, since Mg^{2+} is a divalent ion, it interacts more strongly with the electric field generated by the membrane charges, requires greater charge compensation to maintain electro-neutrality and consequently, its transport is energetically less favourable than that of Li^+. Consequently, Li^+ generally permeates more easily than Mg^{2+}, contributing to the greater rejection of divalent ions observed in nanofiltration membranes. If the

membrane has a weak positive charge, both Li^+ and Mg^{2+} become co-ions and are therefore electrostatically repelled. But, since electrostatic repulsion increases as the ion's valence increases, Mg^{2+} is subjected to greater exclusion than Li^+. Instead, in the case of an electrically neutral membrane, the Donnan effect is essentially absent, and ion transport is primarily governed by the other mechanisms [22], [25], [30].

4.4 Dielectric exclusion

Dielectric exclusion arises from the difference in dielectric constant between the membrane material and the aqueous solution. This difference generates an energy barrier that hinders the entry of ions into the membrane pores [22].

In the pores of NF membranes this phenomenon occurs mainly through two mechanisms. The first is represented by the increase in the energy barrier associated with the transfer of the ion from the bulk of the solution into the pore, due to the reduction of the dielectric constant in the confined spaces, which increases the solvation energy (Born energy) and makes the entry of the ions energetically unfavourable. The second consists of the so-called image forces, generated by the polarization charges induced by the discontinuity of the dielectric constant at the water-membrane interface, which produce a repulsive force proportional to the square of the valence of the ion. Consequently, Mg^{2+} experiences significantly higher dielectric repulsion than Li^+, which contributes to the preferential rejection of divalent ions and enhances Li/Mg separation[25], [29].

Furthermore, some studies have reported that under low pH conditions (a pH of 3.3 was used in laboratory tests) the dielectric exclusion appears to have an improved effect so the separation of Li^+ and Mg^{2+} is increased [30], [31].

4.5 Synergistic interaction between separation mechanisms

Although the small difference in the hydrated radii of Mg^{2+} and Li^+ and the low charge density limit the effectiveness of steric exclusion and the Donnan effect respectively, in commercial membranes, the combined effects of all three mechanisms still allow for effective separation of the two ions. In particular, nanofiltration membranes generally tend to retain divalent cations, increasing the rejection of Mg^{2+} and reducing that of Li^+, favouring the enrichment of the latter in the permeate [22], [23], [25].

Overall, the Li/Mg separation cannot be attributed to a single mechanism, but rather to the synergistic action of steric, electrostatic, and dielectric phenomena. Size selection establishes an initial separation threshold and dielectric exclusion provides the primary discrimination between monovalent and divalent ions. The contribution of the Donnan effect, instead, depends on the membrane's surface charge but generally reinforces the rejection of higher-valent ions. This multiscale cooperation is the foundation of the high performance of nanofiltration membranes in the selective recovery of lithium from brines [25].

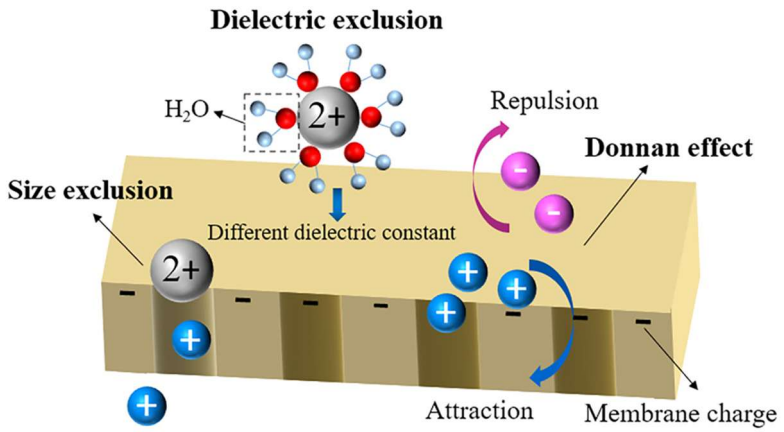


Figure 19. Nanofiltration separation mechanisms for a negatively charged membrane [29].

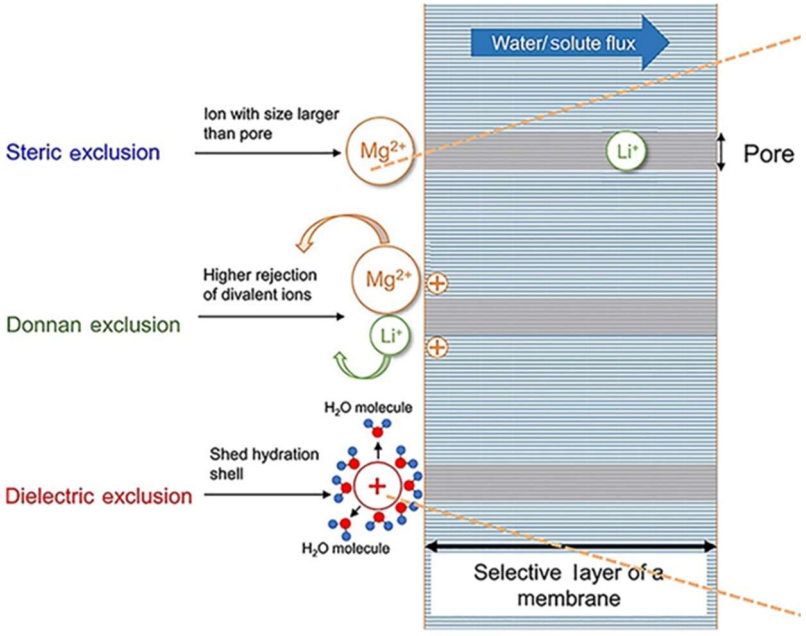


Figure 20. Nanofiltration separation mechanisms for a positively charged membrane [25].

5. Experimental study

5.1 Screening tests on flat-sheet membranes

The first tests conducted were screening tests on flat-sheet membranes, aimed at evaluating the membranes' effectiveness in the selective separation of lithium from magnesium. To this end, the tests were performed using flat-sheet membranes housed in a filtration cell with an active area of 20.6 cm^2.
This experimental phase was divided into three different types of tests:

1. Standard two-step filtration test
2. Standard lithium-magnesium separation test
3. Lithium-magnesium separation tests at variable NaCl concentrations

5.1.1 System and equipment

Before proceeding with the description of the experimental tests, the laboratory setup and the equipment used are presented. This preliminary overview helps establish the experimental context, facilitating understanding of the tests described later and avoiding repetition in the sections dedicated to individual tests.

The equipment
The following is a list of all the equipment used during the laboratory tests.

- Storage tank: it contains the feed, i.e., the solution to be studied in the specific test. During the experiments, the liquid is drawn from the tank, circulated through the system, and returned to this tank.

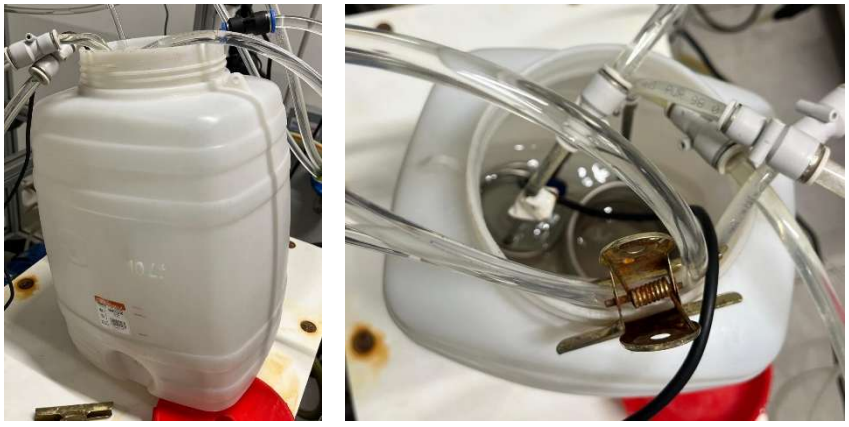


Figure 21. Storage tank, side and top view.

- Pump: its function is to draw the feed solution from the storage tank and circulate it within the experimental system.



Figure 22. Pump

- Three-way valve: it allows the regulation of the system's flow rate, the value of which is monitored by the rotameter.

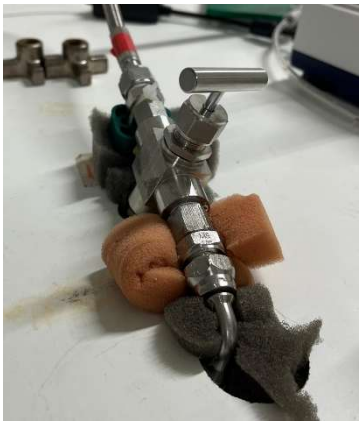


Figure 23. Three-way valve

- Rotameter: a device consisting of a graduated cylinder containing a float that is lifted by the flow of liquid entering from below. The position of the float allows the flow rate of the solution circulating in the system to be determined. In the tests described in this thesis, this parameter will always be maintained at a constant value of approximately 150 L/h.



Figure 24. Rotameter

- Filtration cell: the component that houses the membrane. The cell, which has an active area of 20.6 cm^2, is carefully sealed to ensure the system's integrity and prevent any leaks during tests conducted at relatively high pressures (approximately 20-25 bar).



Figure 25. Closed and open filtration cell.

- Cooling system: used to maintain the solution at the desired temperature.



Figure 26. Cooling system

- Manometer with regulation valve: it allows to monitor and adjust the line pressure, expressed in bar.



Figure 27. Manometer

- Scale and computer: they are connected via cable and used to determine and record permeate flux in LMH. The permeate is collected in a laboratory bottle placed on the scale, with the tubing held in place by a retort stand using a clamp, while a program developed in MATLAB automatically acquires the data through the connection between the scale and the computer.



Figure 28. Scale with laboratory bottle, tube and retort stand using a clamp.

- Digital thermometer: it is used to measure the temperature of solutions in the storage tank.

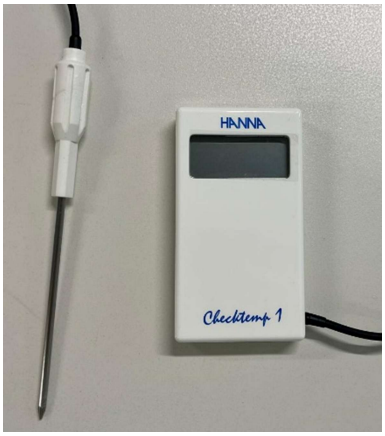


Figure 29. Digital thermometer

- Portable multiparameter meter: it is used to measure the pH and temperature of the solution in the storage tank.



Figure 30. Multiparameter meter and its probe.

- Portable conductivity meter: it is used to measure the conductivity of samples.



Figure 31. Conductivity meter and its probe.

- Magnetic stirrer with stir bar: they're used to ensure that solutions are properly mixed. The system exploits the magnetic coupling between the rotating magnet inside the stirrer and the stir bar immersed in the solution, generating a vortex motion that promotes the mixing of the liquid.

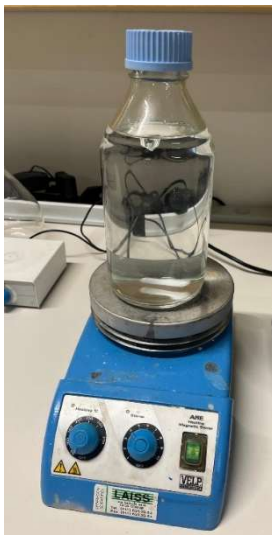


Figure 32. Magnetic stirrer with stir bar inside a laboratory bottle.

- Laboratory bottles and flasks: they're used for preparing, collecting, and transferring the various solutions used during all the tests.

- Manual pipette repeaters and pipette controllers: they're used to accurately measure the volume of solution to be added to the feed in the storage tank in the various tests conducted.

The system

The general operation of the laboratory system begins with filling the storage tank with the feed required for the specific test and preparing the membrane, that is, cutting it to the correct size and making holes in it so it can be inserted into the filtration cell housings. In the latter, the membrane must be oriented with the shiny side, that is the active side, facing the feed inlet side of the cell itself.

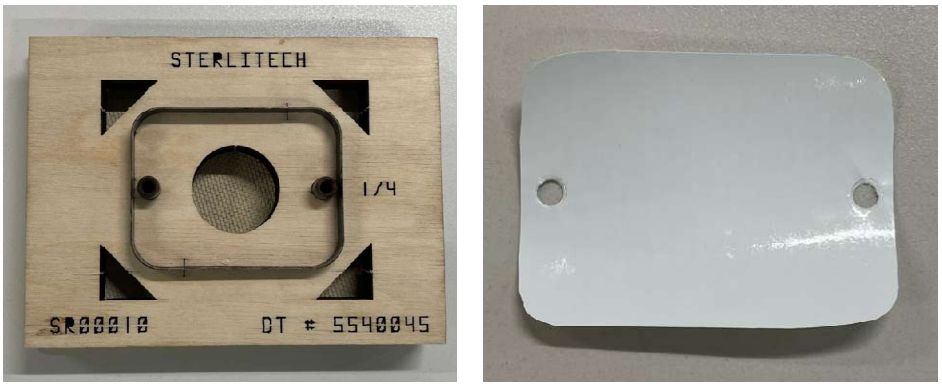


Figure 33. Membrane cutting tool and cut membrane facing the shiny side.

The solution is then drawn in by the pump and circulated throughout the system. After passing through the pump, the flow reaches the three-way valve, which has three connections:

- Inlet line, which carries the fluid from the pump to the valve.
- Outlet line, which supplies the rest of the system.
- Bypass line, which diverts part of the flow directly back to the storage tank, thereby allowing the flow rate within the system to be regulated.

The fluid then reaches the filtration cell containing the membrane, and in this section, the flow is divided in two parts:

- Permeate, consisting of the fraction of the solution that passes through the membrane. This fraction can be collected for subsequent sampling analyses or used to determine the permeate flux using the scale-computer system, after which it is returned to the storage tank.
- Retentate, consisting of the portion of the solution that does not pass through the membrane and continues to flow through the main circuit.

The retentate flow then passes through the manometer and its control valve, and then through the rotameter. Finally, the retentate is returned to the storage tank via a return line, completing the system's closed cycle.

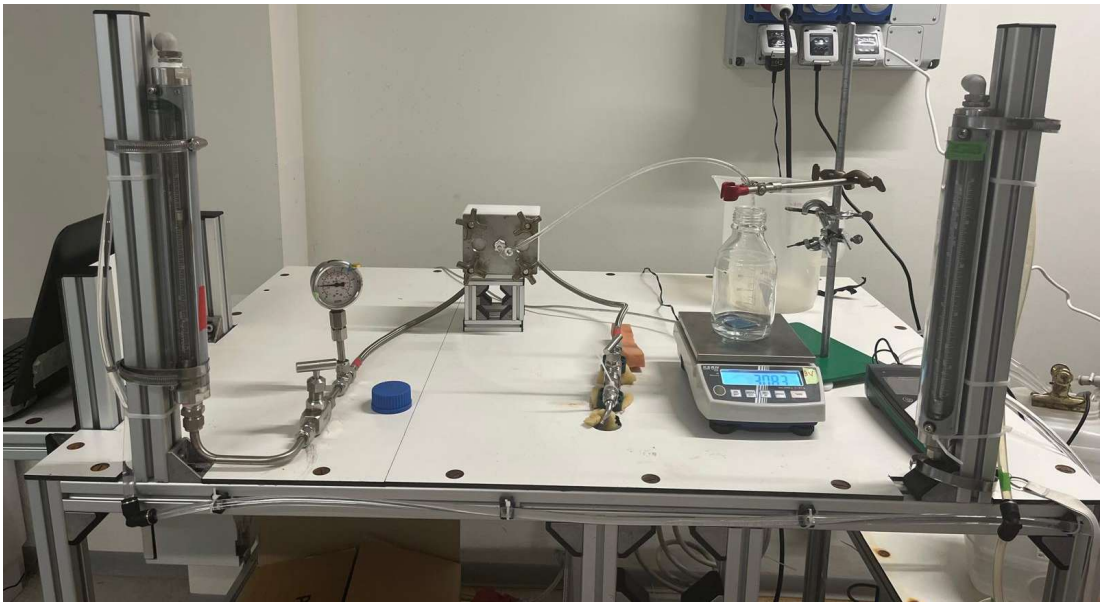


Figure 34. Laboratory system. The image does not show the pump and the cooler, which are located on the floor under the table and on the floor next to the table, respectively.

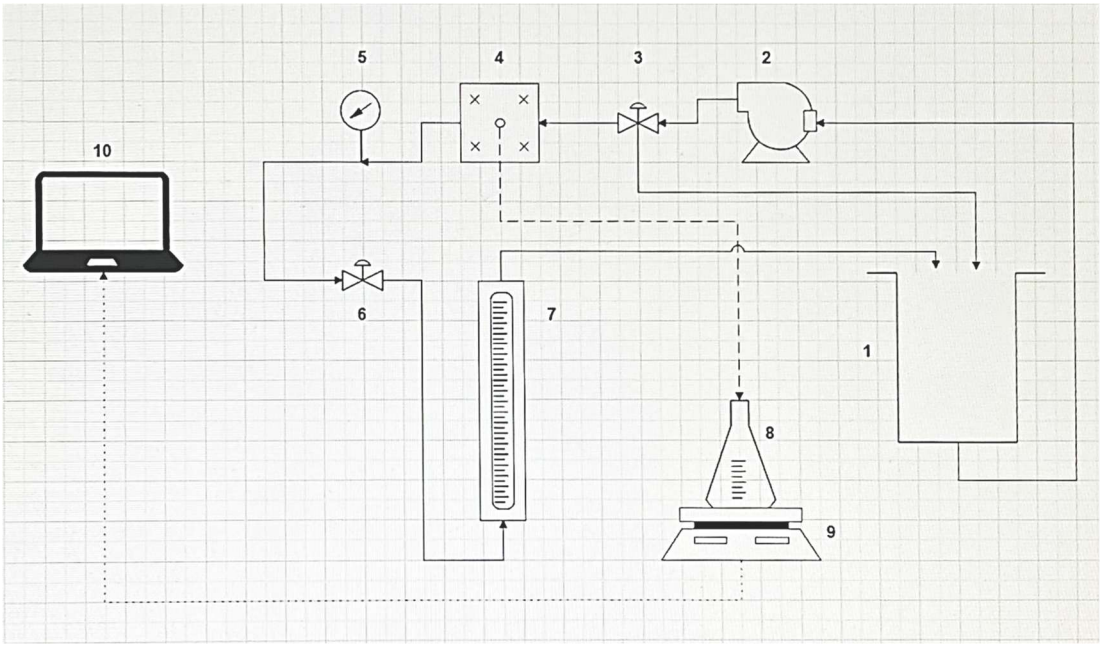


Figure 35. Diagram of the system used in laboratory tests. With (1) storage tank, (2) pump, (3) three-way valve, (4) filtration cell, (5) manometer, (6) manometer regulation valve, (7) rotameter, (8) laboratory bottle, (9) scale and (10) computer.

Washing

An essential step is the cleaning of the laboratory system. This procedure is performed at the end of each test to keep the system in optimal condition, prevent contamination between tests, and thus ensure the reliability of the experimental results.

The cleaning procedure consists of the following steps.

First, the probes of the digital thermometer, the multiparameter meter, and the conductivity meter are carefully rinsed with deionized water and stored in their respective protective cases to ensure they maintain their proper functionality.

Once this step is complete, all laboratory bottles that are no longer needed are placed in the designated dishwasher for the next wash cycle. Flasks containing solutions that are still to be used are sealed with Parafilm and stored properly.

Then, the actual washing of the system begins. The procedure starts by opening the two control valves to reduce the internal pressure to 0 bar. Then, the pump is turned off and the membrane is removed from the filtration cell.

After that, the cell is resealed and the system is configured in open cycle: this means that the recirculation lines that normally return the solution to the storage tank (i.e., the bypass line and the retentate return line) are fed into a larger diameter pipe connected to the sewer system, while the permeate line is directed into the storage tank. By doing so, starting the pump allows for the complete drainage of all the solution present in the system.

Once the drainage is complete, several washing cycles are performed using tap water. The water is fed into the storage tank through a pipe and circulated through the system, still in open configuration, allowing for continuous drainage into the sewer system.

Subsequently, the system is returned to a closed configuration by repositioning all recirculation lines into the storage tank, and in this configuration, additional wash cycles are performed using deionized water.

Once the washing cycle is complete, the system is reconfigured to open mode to allow complete drainage of all liquids.

Finally, the various system components are dried using compressed air.

5.1.2 Test 1: standard two-step filtration test

The objective of this test was to determine the membrane's intrinsic permeance and theoretical selectivity. The first expresses the ability of the filter medium to allow the solvent to pass through it per unit of applied pressure.
Theoretical selectivity, on the other hand, quantifies the membrane's effectiveness in separating or retaining solutes. In the specific case of this test, using a single solute solution of magnesium sulphate ($MgSO_4$), this parameter is represented by the rejection of the salt itself.

The test consists of two main phases: the first involves measuring the permeate flux using a feed of deionized water only, so essentially a hydraulic characterization; the second involves adding a magnesium sulphate solution with a concentration of 2000 ppm to the system and subsequently measuring the permeate flux and conductivity, thereby assessing selectivity.
The operating parameters to be maintained for the test are:

- Applied pressure of 4.8 bar
- Temperature of 25 °C
- pH of 8
- Recovery rate of 0%
  A recovery rate of 0% means continuous recirculation of the feed; in fact, the retentate is returned to the tank, while the volume of permeate removed is so small relative to the system's total capacity that it can be sampled for a short period of time and then returned to the tank itself. In this way, the concentration of magnesium sulphate in the feed remains nearly constant throughout the duration of the test, allowing for the determination of the membrane's intrinsic properties.

The preliminary phase of the test involved calculating the volumes and concentrations required to prepare the two solutions to be used: the first containing magnesium sulphate ($MgSO_4$) for the second phase of the test, and the second containing sodium hydroxide (NaOH) for pH adjustment.

For the first solution, specifically, a final feed volume of 4 L was set, with a $MgSO_4$ concentration of 2000 ppm. Since a concentration of 2000 ppm is equivalent to 2 g/L, the total mass of anhydrous $MgSO_4$ required for each test was 8 g.
However, to facilitate dissolution and mixing, magnesium sulphate heptahydrate ($MgSO_4 \cdot 7H_2O$) was used instead of magnesium sulphate. It was therefore necessary

to perform a stoichiometric conversion based on the respective molecular weights to determine the equivalent amount of hydrated salt to be used.

In addition, the experimental procedure involved the use of a concentrated volume equal to 0.2 L, used to add the solution containing magnesium sulphate heptahydrate foreseen for the second phase of the test, to the 3.8 L of deionized water already introduced into the system for the first phase, thus reaching the target final volume of 4 L. Furthermore, since the same concentrated solution would be used for several consecutive tests, a total stock volume equal to 1 L was prepared, corresponding to five aliquots of 0.2 L each.

Through stoichiometric calculations, the exact amount of hydrated salt to be added to the stock volume was determined, to ensure the desired concentration in the total volume once an aliquot is mixed with it.
The calculations performed are detailed below:

$$initial\ V = 3.8\ L$$

$$added\ V = 0.2\ L$$

$$V = 3.8 + 0.2 = 4\ L$$

$$stock\ V = 1\ L$$

$$MgSO_4\ concentration = 2\ g/L$$

$$m\ MgSO_4 = MgSO_4\ concentration * V = 8\ g$$

$$MW\ MgSO_4 = 120.37\ g/mol$$

$$MW\ MgSO_4.7H_2O = 246.47\ g/mol$$

$$added\ V\ concentration = \frac{m\ MgSO_4}{added\ V} = 40\ g/L$$

$$MgSO_4.7H_2O\ concentration = added\ V\ concentration * \frac{MW\ MgSO_4.7H_2O}{MW\ MgSO_4} =$$

$$= 81.9\ g/L$$

$$m\ MgSO_4.7H_2O = MgSO_4.7H_2O\ concentration * stock\ V = \mathbf{81.9\ g}$$

The next step involved preparing the second solution, a basic solution composed of sodium hydroxide (NaOH), which was needed to raise the pH of the final solution to the required value of 8.

To this end, 10 g of NaOH were dissolved in deionized water, and the solution was then adjusted to volume in a 0.25 L flask. This resulted in a solution with a molar concentration of 1 M (i.e., 1 mol/L).

$$MW\ NaOH = 40 g/mol$$
$$m\ NaOH = 10\ g$$
$$mol\ NaOH = \frac{m\ NaOH}{MW\ NaOH} = 0.25\ mol$$
$$V = 0.25\ L$$
$$molarity = \frac{mol\ NaOH}{V} = 1\ M = 1\ mol/L$$

At this point, it was possible to begin the actual test.
After preparing the system and membrane and checking all the connections, the refrigeration system was activated, set to approximately 14°C to maintain the system temperature at a constant 25°C, measured using a digital thermometer.
The system, as mentioned, was initially fed with a volume of 3.8 L of deionized water. This fluid was used because it contains no salts, does not produce fouling, and does not chemically alter the membrane.

The first operational phase involves membrane compaction, that is a process conducted at a pressure of approximately 20-25 bar for 1.5-2 hours. During this operation, the membrane's active layer undergoes slight compression, the porous substrate structurally settles, and residual internal stresses resulting from manufacturing processes are relaxed, allowing the membrane to achieve a stable structure. From a hydraulic point of view, during this phase, the permeate flux progressively decreases until it stabilizes. It is therefore important to ensure that the flow is constant before proceeding to the subsequent test phases.

Once compaction is complete, the pressure is reduced to 4.8 bar; however, given the sensitivity and resolution of the manometer used in the laboratory, it was decided to maintain a constant pressure of 5 bar. This decrease in pressure also leads to a drop in temperature; consequently, to prevent excessive cooling of the fluid, it was necessary to adjust the operation of the cooling system, increasing its temperature to approximately 22 °C, again to maintain the temperature of the entire system at 25 °C. Then, after emptying the permeate tube, the permeate flux was measured in LMH. Data acquisition was managed using a MATLAB script, which allowed for the

recording of a series of stable values under conditions of constant pressure of 5 bar, with a two-minute time interval.

At this point, the remaining volume was added, i.e., the 200 mL of the volume to be added containing the heptahydrate form of magnesium sulphate.
After the solute was added, the temperature and pH parameters were monitored using a multiparameter meter placed directly in the storage tank. Since the test requires maintaining a pH of 8, it was necessary to correct the pH by adding a quantity of basic NaOH solution in the order of hundreds of μL directly into the tank.

Once the temperature and pH parameters have been verified, for this second phase too it is necessary to wait for the permeate flux values to reach stability and to record them as in the previous case using the MATLAB program.

Subsequently, the sampling phase was carried out to determine the conductivity: specifically, three consecutive permeate samples and one feed sample were taken. The conductivity was then measured in Siemens (S) using a conductivity meter, taking care to carefully rinse it with deionized water after each measurement to avoid altering the results.

In order to ensure data reproducibility and reduce experimental uncertainty, the entire test was performed in duplicate for each of the studied membranes.

5.1.3 Test 2: standard lithium–magnesium separation test

The aim of this second test is to evaluate the ability of the membrane under examination to selectively separate lithium ions (Li^+) from magnesium ions (Mg^{2+}), determining its performance in terms of selectivity and permeation.

The tests are conducted keeping the following operating parameters constant:

- Feed solution containing 4000 mg/L of Mg^{2+} and 500 mg/L of Li^+, introduced respectively in the form of $MgCl_2$ and LiCl
- Temperature of 25 °C
- pH of 3.3
- Recovery of 0%
- Permeate flux of 15 LMH i.e., L/(m^2h)

Before proceeding with the experiment, as for the previously described test, it is necessary to prepare all the solutions required for carrying out the experiment.

The first solution to be prepared is the feed solution containing lithium and magnesium ions, which will be introduced directly into the feed at the beginning of each experimental trial.
Enough solution was prepared to perform three tests (two plus one reserve). It was therefore decided to prepare a concentrated stock solution with a volume of 1 L. Furthermore, the volume present in the storage tank for this test will be 3 L, so the total volume for three tests will be 9 L.
Again, to facilitate the dissolution and mixing of the solution, anhydrous magnesium chloride ($MgCl_2$) was not used, instead its hexahydrate form, magnesium chloride hexahydrate ($MgCl_2 \cdot 6H_2O$), was employed. Consequently, a stoichiometric conversion was necessary to determine the equivalent mass of hydrated salt to be used, in order to ensure the correct concentration of magnesium required in the feed.
The following details the calculations made to determine the quantities of reagents required to prepare the stock solution.
These calculations were developed to obtain the lithium and magnesium concentrations required for the test operating conditions by diluting one-third of the prepared lithium-magnesium solution (equal to 333 mL) in the storage tank until a final volume of 3 L was reached.

$$total\ V = 9\ L$$

$$stock\ V = 1\ L$$

$$Mg\ concentration = 4000\ mg/L$$

$$Li\ concentration = 500\ mg/L$$

$$MW\ Mg = 24.31\ g/mol$$

$$MW\ Li = 6.94\ g/mol$$

$$MW\ MgCl_2.6H_2O = 203.31\ g/mol$$

$$MW\ LiCl = 42.39\ g/mol$$

$$\frac{MW\ MgCl_2.6H_2O}{MW\ Mg} = 8.36$$

$$\frac{MW\ LiCl}{MW\ Li} = 6.11$$

$$m\ MgCl_2.6H_2O = Mg\ concentration * \frac{MW\ MgCl_2.6H_2O}{MW\ Mg} * total\ V$$

$$= \mathbf{301076.10\ mg}$$

$$m\ LiCl = Li\ concentration * \frac{MW\ LiCl}{MW\ Li} * total\ V = \mathbf{27486.31\ mg}$$

$$stock\ V\ MgCl_2.6H_2O\ concentration = \frac{m\ MgCl_2.6H_2O}{stock\ V} = 301076.10\ mg/L$$

$$stock\ V\ LiCl\ concentration = \frac{m\ LiCl}{stock\ V} = 27486.31\ mg/L$$

$$stock\ V\ Mg\ concentration = \frac{stock\ V\ MgCl_2.6H_2O\ concentration}{\frac{MW\ MgCl_2.6H_2O}{MW\ Mg}}$$

$$= 36000\ mg/L$$

$$stock\ V\ Li\ concentration = \frac{stock\ V\ LiCl\ concentration}{\frac{MW\ LiCl}{MW\ Li}} = 4500\ mg/L$$

The second solution prepared is a hydrochloric acid (HCl) solution, used to adjust the pH of the feed solution and maintain it constant at approximately 3.3 throughout the test.

The solution was prepared by mixing 19.28 g of HCl with 230.72 g of deionized water, resulting in a solution with a molar concentration of 2.14 M.

$$m\ HCl = 19.28\ g$$

$$\rho\ HCl = 1.19\ g/ml$$

$$V\ HCl = \frac{m\ HCl}{\rho\ HCl} = 16.20\ ml$$

$$V\ H_2O = 230.72\ ml$$

$$V = V\ HCl + V\ H_2O = 246.92\ ml$$

$$MW\ HCl = 36.46\ g/mol$$

$$mol\ HCl = \frac{m\ HCl}{MW\ HCl} = 0.53\ mol$$

$$molarity = \frac{mol\ HCl}{V/1000} = 2.14\ M\ (= mol/L)$$

Once the solution preparation was complete, the test could proceed. First, all system connections were checked to ensure they were properly closed to prevent any leaks during operation. Next, the membrane was prepared and installed inside the filtration cell. The cooling system was then activated and set to a temperature of approximately 15°C, maintaining the feed solution temperature at 25°C throughout the test. Finally, the scale was connected to the computer and the MATLAB script, used to measure and record the permeate flux, was launched.

Initially, 2 L of deionized water are introduced into the storage tank. The system is then started in a closed-loop configuration by activating the pump and kept running for 30 to 60 minutes to allow the membrane to compact.
Once this preliminary step is completed, one-third of the previously prepared lithium and magnesium stock solution is added to the storage tank, corresponding to a volume of 333 mL. The total volume of the solution is then brought to 3 L by adding an additional 667 mL of deionized water.
After preparing the feed solution, the system is left to recirculate for a few minutes, to promote complete mixing of the components and ensure homogenization of the solution before starting the subsequent experimental operations.

Unlike the first test described, in this one, the permeate flux must be maintained at a constant value of 15 LMH. To this end, the operating pressure is adjusted using the appropriate valve until the desired flow rate is reached. Once the correct operating conditions have been set, the system is left to operate for the time necessary for the

permeate flux and pressure to stabilize, thus ensuring a steady state is reached before measurements and sampling begin.
This stabilization is verified using the MATLAB program, which acquires and records the permeate flux at two-minute intervals. Before proceeding with the subsequent test phases, the measurements must show sufficiently stable values over time.
Subsequently, the temperature and pH values of the feed solution are monitored using a multiparameter meter immersed directly in the storage tank. Specifically, the pH is adjusted to approximately 3.3 by adding the previously prepared HCl solution. Typically, the quantities of acid solution required for this adjustment are on the order of a few thousand microliters (μL).

After a further short waiting period, necessary to guarantee complete stabilization of the conditions following the pH correction, the pH, the temperature (T) and the pressure (p) values present at the time of sampling are recorded.
Then, feed and permeate samples are taken for subsequent analyses. Permeate sampling is carried out directly from the permeate stream exiting the filtration cell, while the feed sample is taken from the storage tank.

At this point, the standard lithium–magnesium separation test could be considered complete. However, in this experimental activity, it is performed in combination with the subsequent lithium–magnesium separation test at variable NaCl concentrations, described in the next paragraph. The latter, in fact, is based on the same operating conditions and the same experimental setup, differing only in some additional steps related to the variation of salinity through the addition of sodium chloride (NaCl) to the solution in the storage tank.

5.1.4 Test 3: lithium–magnesium separation tests at variable NaCl concentrations

The objective of this test is to evaluate the influence of salinity, induced by the presence of sodium chloride (NaCl), on membrane performance in separating lithium and magnesium.

In real saline solutions, lithium and magnesium are not the only ions present in solution. Sodium chloride is often the predominant component and can significantly influence transport phenomena across the membrane. Therefore, it is essential to analyse the system's behaviour under conditions more representative of real-world applications.

Therefore, the test is aimed at evaluating:

- Whether increasing the Na^+ ion concentration interferes with lithium recovery.
- The effect of salinity on the membrane' selectivity for Li/Mg separation.
- The membrane's transport preference for different ionic species in the solution.

According to the experimental protocol adopted, the salinity of the feed is progressively increased by adding sodium chloride (NaCl). The test is divided into five successive steps, defined based on the increase in sodium ion (Na^+) concentration. Specifically, the target Na^+ concentrations considered in the various steps are 1250 mg/L, 2500 mg/L, 5000 mg/L, 10000 mg/L, and 20000 mg/L.

The test operating parameters remain unchanged from those adopted for the standard lithium–magnesium separation test:

- Feed solution containing 4000 mg/L of Mg^{2+} and 500 mg/L of Li^+, introduced respectively in the form of $MgCl_2$ and LiCl
- Temperature of 25 °C
- pH of 3.3
- Recovery of 0%
- Permeate flux of 15 LMH i.e., L/(m^2h)

At this point, it is necessary to determine the quantities of sodium chloride to add for each experimental step, in order to achieve the increments in sodium ion (Na^+) concentration required by the test protocol.

The calculations performed are shown below.

$$MW\ Na = 23\ g/mol$$

$$MW\ NaCl = 58.44\ g/mol$$

$$\frac{MW\ NaCl}{MW\ Na} = 2.54$$

$$Na\ concentrations = 1250 \div 20000\ mg/L$$

$$mg\ NaCl\ (for\ 1L\ solution) = \frac{MW\ NaCl}{MW\ Na} * Na\ concentrations$$

$$storage\ V = 3\ L$$

$$mg\ NaCl\ (for\ 3L\ solution) = mg\ NaCl\ (for\ 1L\ solution) * storage\ V$$

$$mg\ NaCl\ (to\ add\ for\ each\ step) = mg\ NaCl\ (for\ 3L\ solution)\ current\ step +$$

$$- mg\ NaCl\ (for\ 3L\ solution)\ previous\ step$$

This test therefore begins immediately after the previous test ends, which is why the latter can be considered step 0 of this experimental procedure, corresponding to the initial condition without added NaCl.
So, once the feed and permeate sampling for step 0 are completed, the first amount of NaCl can be added.

The addition of NaCl must be done without significantly changing the overall volume of the solution in the storage tank, which must be kept at 3 L. To this end, a small portion of the solution is taken directly from the circuit using one of the return lines that convey the fluid to the tank. The salt is then dissolved in this portion, and the resulting solution is then reintroduced into the storage tank.
Any small amounts of deionized water used to rinse the funnel or container used to weigh the salt can be added to the solution without compromising the volume balance since it compensates for the volume removed from the system during the feed and permeate sampling operations of the previous step.

After adding the NaCl, the pH value of the feed solution is checked again. Due to the change in feed composition, the pH may increase from the target value; therefore, it is brought back to 3.3 by adding the HCl solution. The quantities required for this correction are on the order of a few hundred microliters (μL).
The system is then left to operate until steady-state conditions are reached: the permeate flux is expected to show a stable trend at 15 LMH in the data acquired and recorded by the MATLAB program.

At this point, the pH, temperature (T), and pressure (p) values are recorded. Subsequently, feed and permeate samples are taken as before.

From this point on, the experimental procedure is repeated according to the previously described methods, progressively increasing the amount of NaCl added to the solution to achieve the subsequent Na^+ concentration levels. For each step, after the salt is added, the pH is adjusted, the permeate flux is stabilized, and the feed and permeate are subsequently sampled.

Furthermore, in order to ensure the reliability and reproducibility of the experimental results, for each membrane both the standard lithium–magnesium separation test and the lithium–magnesium separation test at variable NaCl concentrations are performed in two replicates.

5.2 Samples and labels

The samples taken during the first test, the standard two-step filtration test, as mentioned, were analysed directly at the laboratory.
Differently, the samples collected during tests 2 and test 3, the standard lithium–magnesium separation test and the subsequent lithium–magnesium separation test at variable NaCl concentrations, were analysed by a specialized external laboratory. This choice was made to obtain measurements characterized by the highest possible level of accuracy and precision, essential for a correct evaluation of the membrane's performance.

Furthermore, the total number of samples collected for the second and third tests remains to be specified. Six sampling levels were considered for each, corresponding to steps 0 to 5. At each step, two samples were collected, feed and permeate. The entire procedure was also performed in duplicate and repeated on two different membranes. Consequently, the total number of samples collected is 48.

A labelling system was then developed for managing and shipping the test tubes to the external laboratory. To this end, a dedicated Excel file was created, in which to each sample was assigned a unique identification code.

Subsequently, the theoretical concentrations of Li^+, Mg^{2+}, Na^+ expressed in mg/L were calculated:

- Regarding lithium (Li^+), the initial concentration in the feed was 500 mg/L. Assuming a theoretical rejection of 20%, the resulting theoretical concentration in the permeate, constant for all steps, is equal to:

$$500 * \frac{100 - 20}{100} = 400\ mg/L$$

- For magnesium (Mg^{2+}), the initial concentration in the feed was 4000 mg/L. Assuming a theoretical rejection of 90%, the resulting theoretical concentration in the permeate, constant for all steps, is equal to:

$$4000 * \frac{100 - 90}{100} = 400\ mg/L$$

- Finally, regarding sodium (Na^+), the initial concentration in the feed varied from 0 to 20000 mg/L, depending on the sampling step considered. Assuming

a theoretical rejection of 10%, the resulting theoretical concentration in the permeate is equal to:

$$step\ 0{:}\ 0 * \frac{100-10}{100} = 0\ mg/L$$
$$step\ 1{:}\ 1250 * \frac{100-10}{100} = 1125\ mg/L$$
$$step\ 2{:}\ 2500 * \frac{100-10}{100} = 2250\ mg/L$$
$$step\ 3{:}\ 5000 * \frac{100-10}{100} = 4500\ mg/L$$
$$step\ 4{:}\ 10000 * \frac{100-10}{100} = 9000\ mg/L$$
$$step\ 5{:}\ 20000 * \frac{100-10}{100} = 18000\ mg/L$$

The theoretical salinity was then also determined, using the results obtained from the calculations described above and according to the following expression:

$$Total\ salinity\ \left(\frac{mg}{L}\right) =$$
$$= Li^{+}\left(\frac{mg}{L}\right) * \frac{LiCl}{Li} + Mg^{2+}\left(\frac{mg}{L}\right) * \frac{MgCl_2.6H_2O}{Mg} + Na^{+}\left(\frac{mg}{L}\right) * \frac{NaCl}{Na}$$

To calculate the salinity of the feed, the following term, relating to HCl, has also been added to the previous formula, which however does not affect the total salinity:

$$total\ HCl\ added\ until\ the\ current\ step\ (mol) * MW\ HCl$$

Afterwards, all the obtained values were organized and linked to the respective sample identification code. All this information was then structured in label format, printed, and applied to the corresponding test tubes. The labelled test tubes were finally packaged and shipped to the external laboratory responsible for the analyses, which will analyse their contents to verify the correct quantities of the values calculated only theoretically.

Below is reported an example of the first replicate of the TS50 membrane.

Code (Long version)	Code (short version)	Total salinity (mg/L)	Li+ (mg/L)	Mg2+ (mg/L)	Na+ (mg/L)	HCl (mol)
TS50-Na steps-Replicate1-F0	BAF1-0	36507	500	4000	0	0.007
TS50-Na steps-Replicate1-F1	BAF1-1	39685	500	4000	1250	0.008
TS50-Na steps-Replicate1-F2	BAF1-2	42862	500	4000	2500	0.009
TS50-Na steps-Replicate1-F3	BAF1-3	49217	500	4000	5000	0.010
TS50-Na steps-Replicate1-F4	BAF1-4	61927	500	4000	10000	0.012
TS50-Na steps-Replicate1-F5	BAF1-5	87347	500	4000	20000	0.014
TS50-Na steps-Replicate1-P0	BAP1-0	5789	400	400	0	
TS50-Na steps-Replicate1-P1	BAP1-1	8648	400	400	1125	
TS50-Na steps-Replicate1-P2	BAP1-2	11508	400	400	2250	
TS50-Na steps-Replicate1-P3	BAP1-3	17227	400	400	4500	
TS50-Na steps-Replicate1-P4	BAP1-4	28666	400	400	9000	
TS50-Na steps-Replicate1-P5	BAP1-5	51544	400	400	18000	

Figure 36. Coding and calculation example for the replica 1 of the TS50 membrane.

Label
Code:BAF1-0; Li: 500 (mg/L); Mg: 4000 (mg/L); Na: 0 (mg/L); Total salinity: 36507 (mg/L)
Code:BAF1-1; Li: 500 (mg/L); Mg: 4000 (mg/L); Na: 1250 (mg/L); Total salinity: 39685 (mg/L)
Code:BAF1-2; Li: 500 (mg/L); Mg: 4000 (mg/L); Na: 2500 (mg/L); Total salinity: 42862 (mg/L)
Code:BAF1-3; Li: 500 (mg/L); Mg: 4000 (mg/L); Na: 5000 (mg/L); Total salinity: 49217 (mg/L)
Code:BAF1-4; Li: 500 (mg/L); Mg: 4000 (mg/L); Na: 10000 (mg/L); Total salinity: 61927 (mg/L)
Code:BAF1-5; Li: 500 (mg/L); Mg: 4000 (mg/L); Na: 20000 (mg/L); Total salinity: 87347 (mg/L)
Code:BAP1-0; Li: 400 (mg/L); Mg: 400 (mg/L); Na: 0 (mg/L); Total salinity: 5789 (mg/L)
Code:BAP1-1; Li: 400 (mg/L); Mg: 400 (mg/L); Na: 1125 (mg/L); Total salinity: 8648 (mg/L)
Code:BAP1-2; Li: 400 (mg/L); Mg: 400 (mg/L); Na: 2250 (mg/L); Total salinity: 11508 (mg/L)
Code:BAP1-3; Li: 400 (mg/L); Mg: 400 (mg/L); Na: 4500 (mg/L); Total salinity: 17227(mg/L)
Code:BAP1-4; Li: 400 (mg/L); Mg: 400 (mg/L); Na: 9000 (mg/L); Total salinity: 28666 (mg/L)
Code:BAP1-5; Li: 400 (mg/L); Mg: 400 (mg/L); Na: 18000 (mg/L); Total salinity: 51544 (mg/L)

Figure 37. Label example for the replica 1 of the TS50 membrane.

6. Data and results

6.1 Test 1: standard two-step filtration test

The objective of this test was to determine the intrinsic permeance and the theoretical selectivity of the membranes.

6.1.1 Collected data

Following the experimental tests, the MATLAB software generated a file containing the recorded data on acquisition time (min) and permeate flux (LMH) for both phases of the test: an initial phase conducted using only deionized water (DI), and a second phase performed after the addition of the magnesium sulphate ($MgSO_4$) solution.
The flux data are reported in the tables below.

Table 2. Averaged permeate flux data acquired with MATLAB and related standard deviation for both replicates of the TS50 membrane and both phases of the test.

	DI		**$MgSO_4$**	
TS50	**Average flux (LMH)**	**Standard deviation (LMH)**	**Average flux (LMH)**	**Standard deviation (LMH)**
REP 1	37.91	0.45	29.18	0.77
REP 2	37.70	1.48	27.22	0.50

Table 3. Averaged permeate flux data acquired with MATLAB and related standard deviation for both replicates of the XPNF membrane and both phases of the test.

	DI		**$MgSO_4$**	
XPNF	**Average flux (LMH)**	**Standard deviation (LMH)**	**Average flux (LMH)**	**Standard deviation (LMH)**
REP 1	31.76	0.43	26.24	0.57
REP 2	33.15	0.61	27.31	0.76

Intrinsic permeance

Intrinsic permeance was calculated using the flux values obtained in the first phase of the test, as the use of deionized water allows for the evaluation of the membrane's hydraulic performance. Permeance was determined by dividing the permeate flux by the transmembrane pressure applied during the experiment, equal to 5 bar, according to the following relationship:

$$Permeance\ (LMH/bar) = \frac{flux\ (LMH)}{pressure\ (bar)}$$

For each membrane and experimental replicate, the average permeance value and the related standard deviation were calculated and reported in the following tables.

Table 4. Calculated average permeance and related standard deviation for both replicates of the TS50 membrane.

TS50	**Average permeance (LMH/bar)**	**Standard deviation (LMH/bar)**
REP 1	7.58	0.09
REP 2	7.54	0.29

Table 5. Calculated average permeance and related standard deviation for both replicates of the XPNF membrane.

XPNF	**Average permeance (LMH/bar)**	**Standard deviation (LMH/bar)**
REP 1	6.35	0.09
REP 2	6.63	0.12

Subsequently, since each membrane was tested in duplicate, the overall mean between the two tests and the corresponding standard deviation were determined, in order to obtain a representative and statistically robust value of the membrane performance. These values are reported in the following table.

Table 6. Average intrinsic permeance of the two replicates for the TS50 and XPNF membranes and the associated standard deviation.

Membrane	**Permeance (LMH/bar)**
TS50	7.56 ± 0.03
XPNF	6.49 ± 0.19

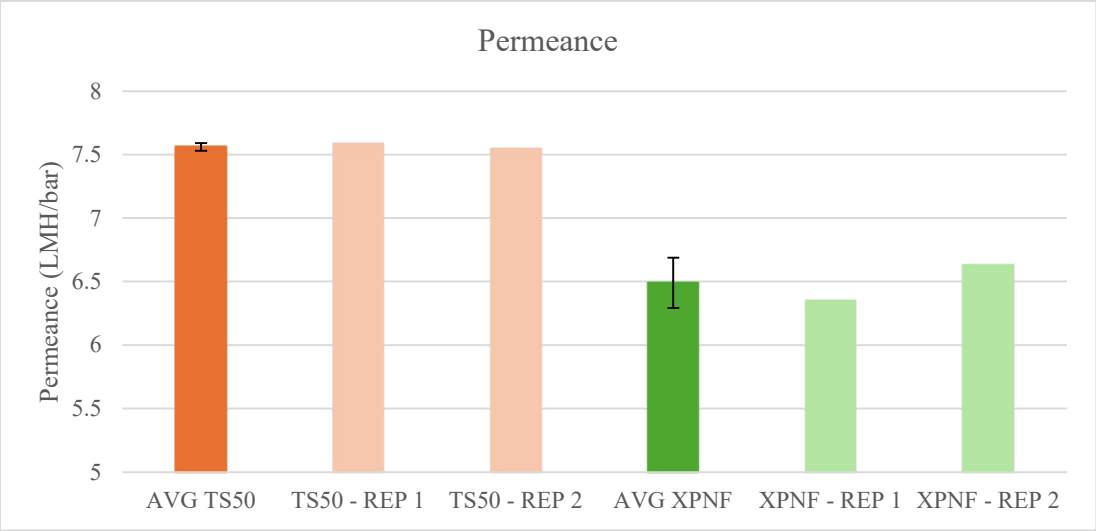


Figure 38. Visual representation of the intrinsic permeance values, showing both replicates and their average for both membranes.

Theoretical selectivity

Once the intrinsic permeance was determined, the theoretical selectivity of the membranes could be evaluated. To this end, the rejection of $MgSO_4$ was used as a representative parameter of the membrane's ability to retain a divalent salt, according to the method commonly used for the characterization and classification of nanofiltration membranes.

Two experimental replicates were performed for each membrane. In each test, the electrical conductivity of the feed solution was measured once, while that of the permeate was measured three consecutive times. These measurements allowed the $MgSO_4$ rejection to be calculated using the following relationship:

$$Rejection\ (\%) = \left(1 - \frac{electrical\ conductivity\ in\ permeate}{electrical\ conductivity\ in\ feed}\right) * 100$$

So, for each replicate, three rejection values were obtained, from which the average rejection and the corresponding standard deviation were calculated.
The data and results of these tests are shown in the following tables:

Table 7. Electrical conductivity values measured once for the feed and three times for the permeate, rejection values calculated for all three permeate measurements, average rejection value and its standard deviation for replicate 1 of the TS50 membrane.

TS50 REP 1	Electrical conductivity (mS/cm)	Rejection rate (%)	Average rejection (%)	Standard deviation (%)
Feed	2.10	-	-	-
Permeate 1	0.015	99.31	99.30	0.02
Permeate 2	0.015	99.28		
Permeate 3	0.014	99.32		

Table 8. Electrical conductivity values measured once for the feed and three times for the permeate, rejection values calculated for all three permeate measurements, average rejection value and its standard deviation for replicate 2 of the TS50 membrane.

TS50 REP 2	Electrical conductivity (mS/cm)	Rejection rate (%)	Average rejection (%)	Standard deviation (%)
Feed	2.20	-	-	-
Permeate 1	0.022	99.01	99.07	0.05
Permeate 2	0.019	99.10		
Permeate 3	0.020	00.09		

Table 9. Electrical conductivity values measured once for the feed and three times for the permeate, rejection values calculated for all three permeate measurements, average rejection value and its standard deviation for replicate 1 of the XPNF membrane.

XPNF REP 1	Electrical conductivity (mS/cm)	Rejection rate (%)	Average rejection (%)	Standard deviation (%)
Feed	2.3	-	-	-
Permeate 1	0.13	94.35	94.57	0.20
Permeate 2	0.12	94.74		
Permeate 3	0.12	94.63		

Table 10. Electrical conductivity values measured once for the feed and three times for the permeate, rejection values calculated for all three permeate measurements, average rejection value and its standard deviation for replicate 2 of the XPNF membrane.

XPNF REP 2	Electrical conductivity (mS/cm)	Rejection rate (%)	Average rejection (%)	Standard deviation (%)
Feed	2.1	-	-	-
Permeate 1	0.16	92.19	91.88	0.26
Permeate 2	0.17	91.76		
Permeate 3	0.17	91.71		

Subsequently, similarly to what was performed for intrinsic permeance, the results of the two replicates were combined by calculating the overall average and the corresponding standard deviation, in order to obtain a single value representative of the rejection of each membrane.

These rejection values obtained for the TS50 and XPNF membranes are shown below.

Table 11. Average theoretical selectivity of the two replicates for the TS50 and XPNF membranes and the associated standard deviation.

Membrane	MgSO4 rejection (%)
TS50	99.18 ± 0.16
XPNF	93.23 ± 1.89

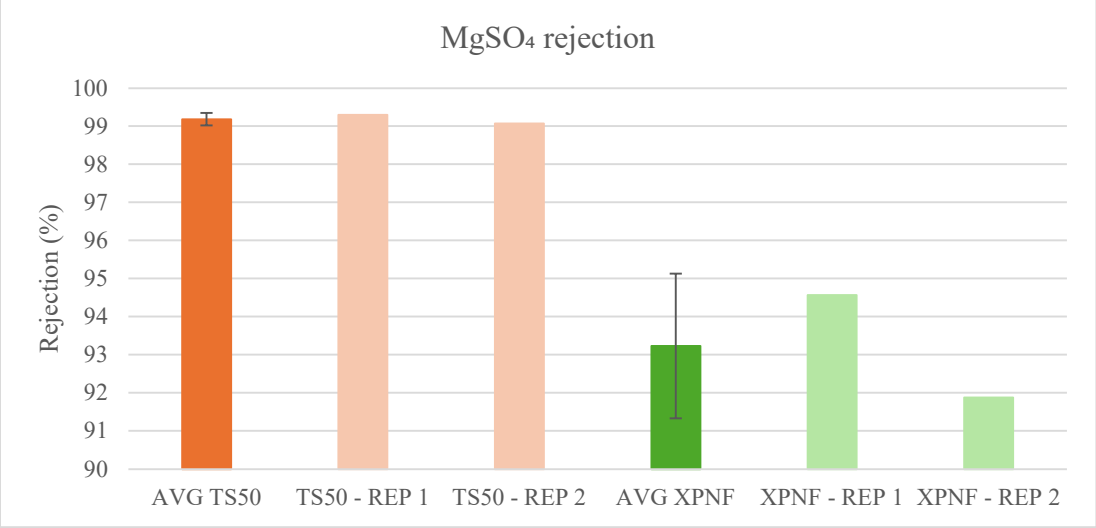


Figure 39. Visual representation of the theoretical selectivity values, showing both replicates and their average for both membranes.

6.1.2 Results interpretation

The results obtained highlight significant differences between the two membranes investigated. The TS50 showed a higher intrinsic permeance (7.56 ± 0.03) than the XPNF (6.49 ± 0.19), indicating lower hydraulic resistance to water transport and, consequently, higher productivity at the same applied pressure. At the same time, the TS50 also showed significantly higher $MgSO_4$ rejection (99.18 ± 0.16) than the XPNF (93.23 ± 1.89), indicating a greater capacity to retain divalent ionic species.

Unlike what is commonly observed in nanofiltration membranes, where an increase in permeability is often accompanied by a reduction in selectivity, in this case the TS50 showed superior performance in both parameters. This suggests that the membrane possesses a more efficient selective layer structure, capable of promoting water transport while simultaneously limiting the passage of $MgSO_4$ ions.

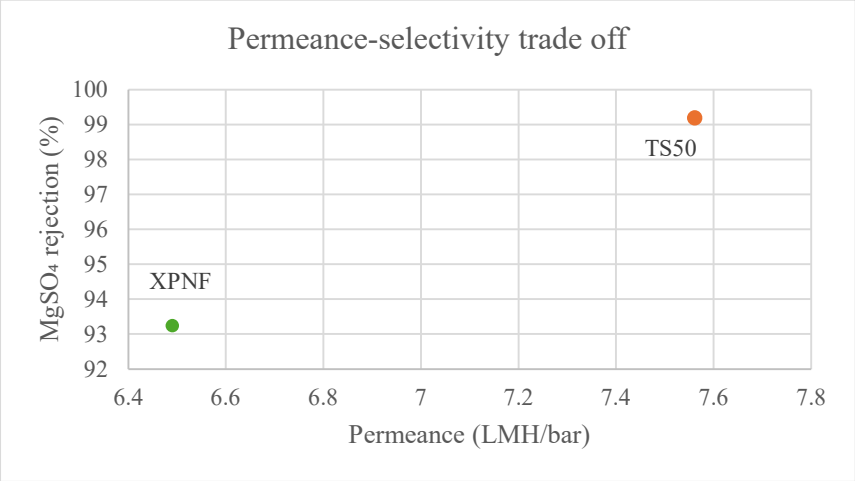


Figure 40. Graphical representation of the correlation between permeance and selectivity performance, showing the average values of both parameters for both membranes.

The presence of a higher surface charge density and/or a more compact structure of the TS50 active layer could have intensified the salt retention phenomena. Based on these results, the TS50 appears to be the membrane with the best performance in the preliminary characterization test.

6.2 Test 2: standard lithium–magnesium separation test

The aim of this second test is to evaluate the ability of nanofiltration membranes to selectively separate lithium ions (Li^+) from magnesium ions (Mg^{2+}), determining their separation performance.

This second Li/Mg separation test was therefore conducted to verify the membranes' ability to facilitate the passage of lithium ions through the membrane while simultaneously retaining magnesium ions. Unlike the preliminary test with $MgSO_4$, which aimed to generally characterize the membranes' permeability and selectivity properties, this test reproduces conditions more representative of a real lithium recovery process from solutions, allowing for a direct assessment of the membrane's effectiveness in separating the two cations of interest.

6.2.1 Collected data

The permeate flux values, expressed in LMH, were acquired using the MATLAB software during the entire duration of the test. For each experiment, the average values and the relative standard deviation were subsequently calculated and these values are reported in the following tables.

Table 12. Averaged permeate flux data acquired with MATLAB and related standard deviation for both replicates of the TS50 membrane.

TS50	Average flux (LMH)	Standard deviation (LMH)
REP 1	14.50	0.57
REP 2	15.40	0.25

Table 13. Averaged permeate flux data acquired with MATLAB and related standard deviation for both replicates of the XPNF membrane.

XPNF	Average flux (LMH)	Standard deviation (LMH)
REP 1	15.01	1.07
REP 2	13.85	0.72

Instead, the data relating to the concentrations of lithium and magnesium ions and the salinity of the feed and permeate solutions were obtained from chemical analyses performed on the samples taken during the experimental tests by a specialized external laboratory.

The results obtained from the analyses are reported below.

Table 14. Concentrations of lithium, magnesium and sodium ions and salinity of the feed and permeate solutions for both replicates of the TS50 membrane.

TS50	Salinity (mg/L)	Li^+ (mg/L)	Mg^{2+} (mg/L)	Na^+ (mg/L)
REP 1 - feed	36507	607	5002	2
REP 1 - permeate	5789	665	99	2
REP 2 - feed	36507	525	4300	4
REP 2 - permeate	5789	516	70	3

Table 15. Concentrations of lithium, magnesium and sodium ions and salinity of the feed and permeate solutions for both replicates of the XPNF membrane.

XPNF	Salinity (mg/L)	Li^+ (mg/L)	Mg^{2+} (mg/L)	Na^+ (mg/L)
REP 1 - feed	36507	554	4546	4
REP 1 - permeate	5789	542	425	4
REP 2 - feed	36507	534	4345	10
REP 2 - permeate	5789	630	514	59

Starting from these experimental data obtained from the analyses, the main parameters used to evaluate the membrane performance in the Li/Mg separation were calculated as follows:

- Actual ionic strength

$$I\ (mM) = \frac{1}{2}\sum c_i * {z_i}^2$$

where c_i represents the molar concentration of the i-th ion and z_i its charge (i.e. valence).

- Lithium observed rejection rate

$$R_{Li} = 1 - \frac{C_{Li\ permeate}}{C_{Li\ feed}}$$

- Magnesium observed rejection rate

$$R_{Mg} = 1 - \frac{C_{Mg\ permeate}}{C_{Mg\ feed}}$$

- Li, Mg separation factor

$$S_{Li,Mg} = \frac{\frac{C_{Li\ permeate}}{C_{Li\ feed}}}{\frac{C_{Mg\ permeate}}{C_{Mg\ feed}}}$$

The obtained values are reported for both membranes and both replicates in the following tables.

Table 16. Calculated values of actual ionic strength (I), lithium rejection rate (R_{Li}), magnesium rejection rate (R_{Mg}) and lithium-magnesium separation factor ($S_{Li, Mg}$) for both replicates of the TS50 membrane.

TS50	**I (mM)**	**R_{Li} (%)**	**R_{Mg} (%)**	**$S_{Li, Mg}$**
REP 1	704.78	-9.65	98.02	55.35
REP 2	606.51	1.77	98.37	60.10

Table 17. Calculated values of actual ionic strength (I), lithium rejection rate (R_{Li}), magnesium rejection rate (R_{Mg}) and lithium-magnesium separation factor ($S_{Li, Mg}$) for both replicates of the XPNF membrane.

XPNF	**I (mM)**	**R_{Li} (%)**	**R_{Mg} (%)**	**$S_{Li, Mg}$**
REP 1	641.02	2.16	90.65	10.47
REP 2	613.71	-17.87	88.17	9.96

Two experimental replicates were so performed for each membrane. The values obtained for the parameters described above were then averaged, and the standard deviation for each parameter was calculated to obtain a result representative of the membrane's performance. These values are reported below.

Table 18. Average permeate flux, actual ionic strength (I), lithium rejection rate (R_{Li}), magnesium rejection rate (R_{Mg}) and lithium-magnesium separation factor ($S_{Li, Mg}$) of the two replicates for the TS50 and XPNF membranes and the associated standard deviations.

	Permeate flux (LMH)	**I (mM)**	**R_{Li} (%)**	**R_{Mg} (%)**	**$S_{Li, Mg}$**
TS50	14.95 ± 0.64	655.65 ± 69.49	-3.94 ± 8.08	98.19 ± 0.25	57.73 ± 3.36
XPNF	14.43 ± 0.82	627.36 ± 19.31	-7.86 ± 14.16	89.41 ± 1.76	10.21 ± 0.36

6.2.2 Results interpretation

Actual ionic strength

Analysing these data, it can be seen that the actual ionic strength is comparable between the two membrane tests, confirming that both experiments were performed under similar chemical conditions. Therefore, the observed differences in lithium and magnesium rejection can be primarily attributed to the intrinsic properties of the membranes rather than to variations in feed composition.

Permeate flux

Furthermore, the permeate flux measurements show very similar values for both membranes (14.95 ± 0.64 LMH for TS50 and 14.43 ± 0.82 LMH for XPNF), confirming that the system operated under stable conditions and close to the target flux value of 15 LMH.

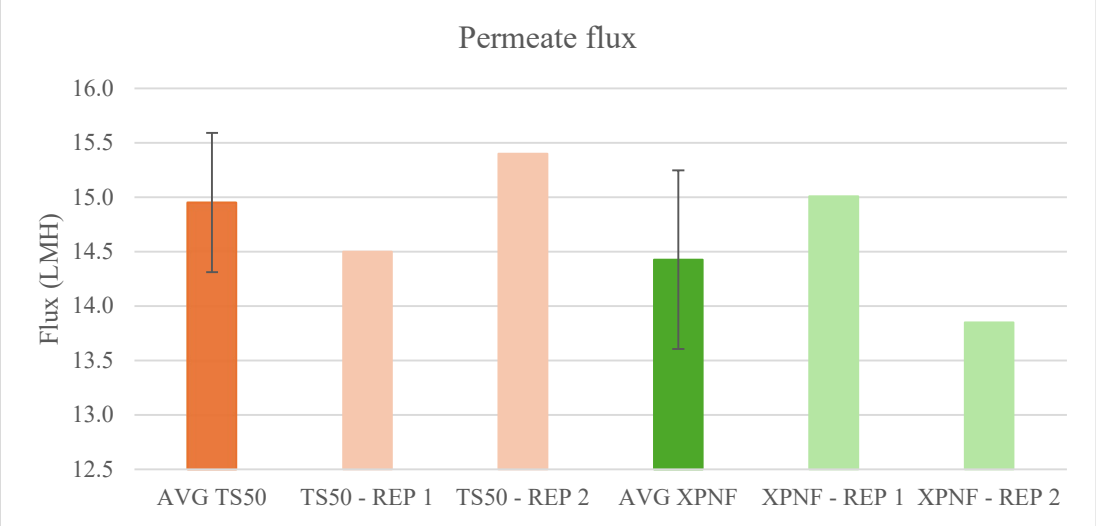


Figure 41. Visual representation of the permeate flux values, showing both replicates and their average for both membranes.

Li rejection

Lithium rejection analysis shows negative values close to zero for both membranes (-3.94 ± 8.08% for TS50 and -7.96 ± 14.16% for XPNF). The presence of negative values is attributable to ion transport phenomena and the electrochemical equilibria established during filtration. From an application point of view, this type of rejection represents a favourable result, as it indicates that lithium easily crosses the membrane, favouring its recovery in the permeate. Furthermore, the high standard deviation observed for this parameter reflects the closeness of the rejection to zero and the limited number of replicates.

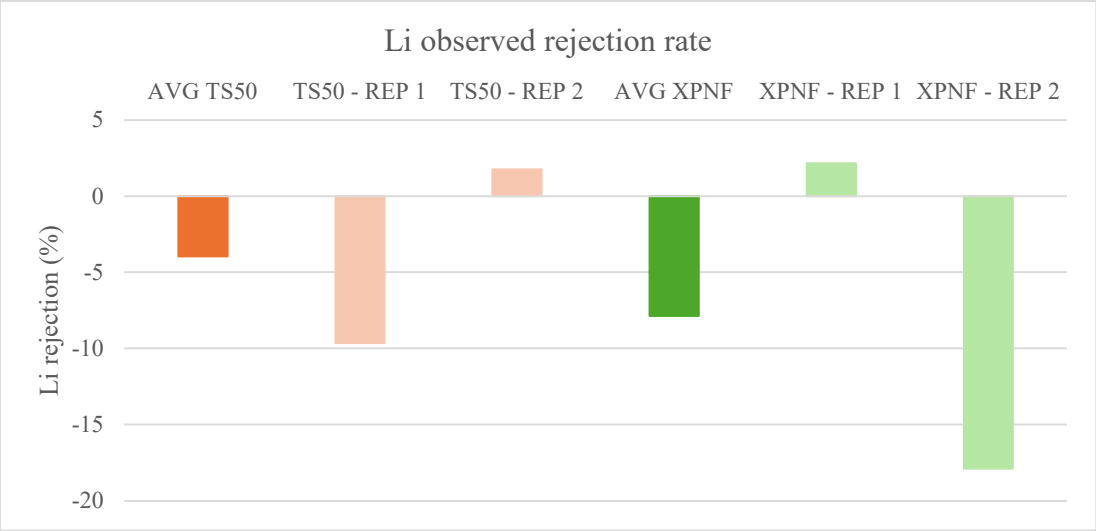


Figure 42. Visual representation of lithium rejection values, showing both replicates and their average for both membranes.

Mg rejection

Regarding magnesium, both membranes show a high retention capacity. However, the TS50 achieves an average rejection of 98.19 ± 0.25%, while the XPNF stands at 89.41 ± 1.76%. This difference highlights the greater effectiveness of the TS50 in retaining Mg^{2+} ions, a behaviour consistent with what was observed in Test 1, where the same membrane had already shown a higher rejection of $MgSO_4$. The greater retention of magnesium can be traced back to the combination of steric exclusion mechanisms, Donnan effect, and dielectric exclusion, which penalize divalent and highly hydrated ions more than monovalent ions such as lithium.

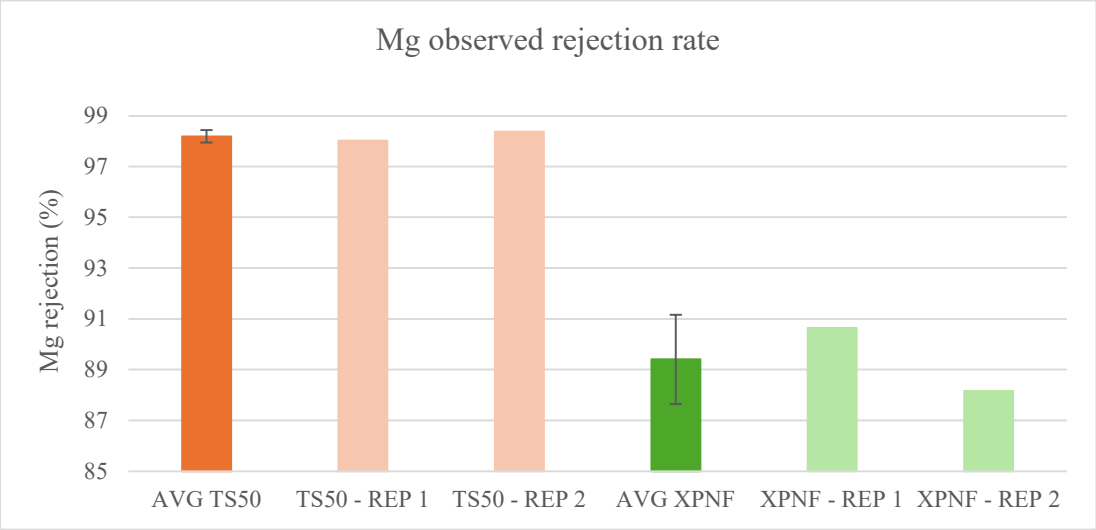


Figure 43. Visual representation of magnesium rejection values, showing both replicates and their average for both membranes.

Lithium-magnesium separation factor

The parameter that summarizes the membrane's overall performance is the Li/Mg separation factor, as it simultaneously takes into account lithium permeation and magnesium retention. The results show a clear superiority of the TS50, which achieves a separation factor of 57.73 ± 3.36, versus 10.21 ± 0.36 for the XPNF.

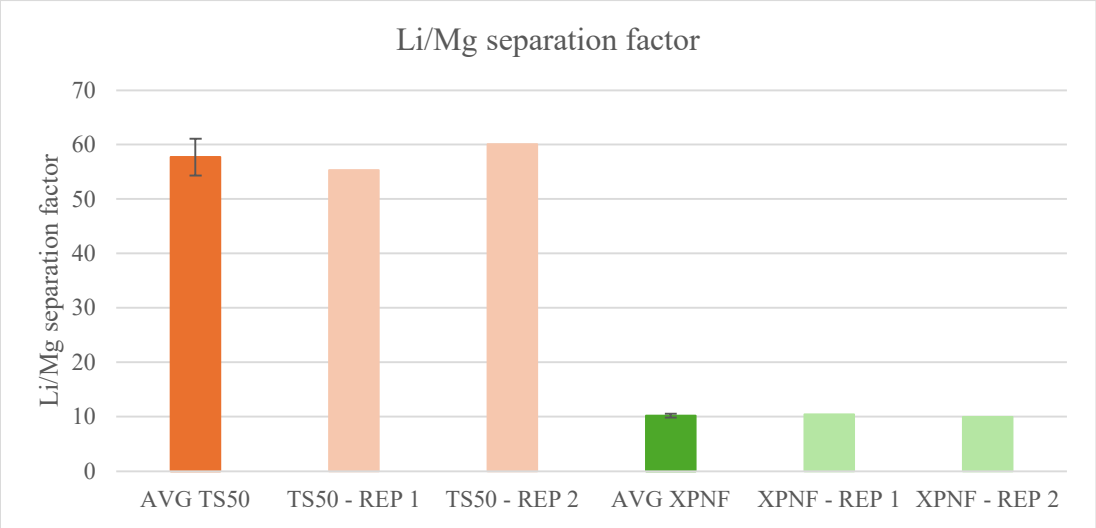


Figure 44. Visual representation of the lithium-magnesium separation factor, showing both replicates and their average for both membranes.

Li and Mg rejection comparison

Considering that both membranes exhibit near-zero lithium rejection, the marked difference in separation factor is mainly due to the TS50's greater capacity to retain magnesium.

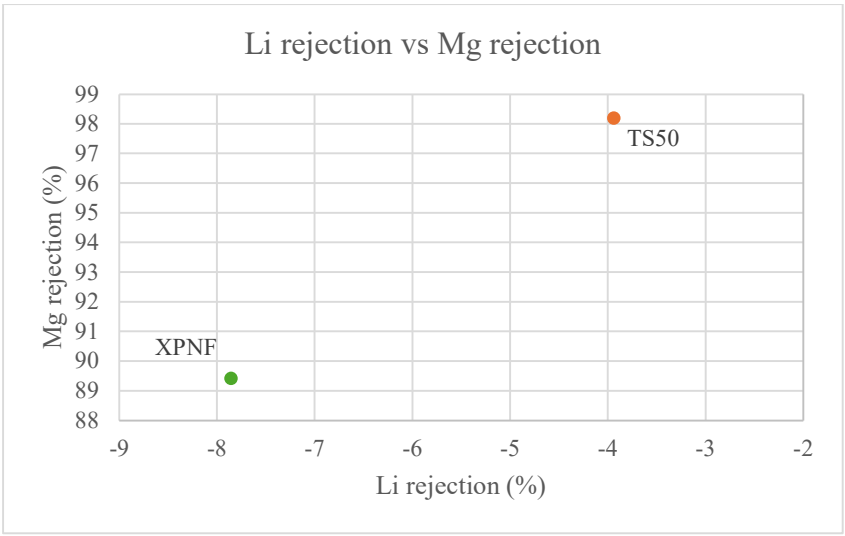


Figure 45. Graphical representation of the correlation between lithium and magnesium rejection performance, showing the average values of both parameters for both membranes.

This indicates that the TS50 achieves a much more effective separation between the two cations, proving, also in this second test, to be the most promising membrane for the selective recovery of lithium.

The comparison with Test 1 also confirms that the best performance in the preliminary characterization of the TS50 also translates into superior performance in Li/Mg separation. In this case, therefore, the high rejection of $MgSO_4$ observed in the screening test proved to be a good indicator of the membrane's ability to retain divalent ions even in a mixture containing lithium and magnesium. However, the decisive parameter remains the Li/Mg separation factor, as it represents the most comprehensive indicator of separation process efficiency and is the primary criterion for membrane selection in lithium recovery applications.

6.3 Test 3: lithium–magnesium separation tests at variable NaCl concentrations

The third test was conducted to evaluate the influence of salinity, induced by the addition of sodium chloride (NaCl), on membrane performance in the selective separation of lithium (Li^+) and magnesium (Mg^{2+}) ions.

To this end, the NaCl concentration in the feed solution was progressively increased from 0 to 20000 mg/L across six experimental steps (from step 0, corresponding to the conditions of Test 2, to step 5). The permeate flux, equal to 15 LMH, temperature (25 °C), pH (3.3), and initial lithium and magnesium concentrations were kept constant throughout the test.

6.3.1 Collected data

As in previous tests, the permeate flux was acquired and recorded using MATLAB software during each test. For each salinity level, the average flux and its standard deviation were then calculated. Furthermore, since the test was conducted at a constant permeate flux, the transmembrane pressure was gradually adjusted to compensate for the increase in transport resistance caused by the rise in salinity. Specifically, in the case of the TS50 membrane, it was necessary to increase the pressure after each addition of NaCl to maintain the target flux.

The flux and pressure values of the different experimental steps are reported in the following tables.

Table 19. Averaged permeate flux data acquired with MATLAB, related standard deviation and measured pressure as salinity increases for replicate 1 of the TS50 membrane.

TS50 - REP 1		
Nominal additional NaCl concentration (mg/L)	**Average flux (LMH)**	**Pressure (bar)**
Step 0: 0	14.50 ± 0.57	12.50
Step 1: 1250	15.90 ± 0.91	13.00
Step 2: 2500	16.55 ± 0.82	13.80
Step 3: 5000	15.74 ± 0.74	13.80
Step 4: 10000	15.58 ± 0.31	14.00
Step 5: 20000	15.37 ± 0.26	15.00

Table 20. Averaged permeate flux data acquired with MATLAB, related standard deviation and measured pressure as salinity increases for replicate 2 of the TS50 membrane.

TS50 - REP 2		
Nominal additional NaCl concentration (mg/L)	**Average flux (LMH)**	**Pressure (bar)**
Step 0: 0	15.40 ± 0.25	12.50
Step 1: 1250	15.12 ± 0.53	12.50
Step 2: 2500	15.59 ± 0.30	12.50
Step 3: 5000	15.19 ± 0.51	12.50
Step 4: 10000	14.98 ± 0.40	14.00
Step 5: 20000	16.00 ± 0.22	15.00

Table 21. Averaged permeate flux data acquired with MATLAB, related standard deviation and measured pressure as salinity increases for replicate 1 of the XPNF membrane.

XPNF - REP 1		
Nominal additional NaCl concentration (mg/L)	**Average flux (LMH)**	**Pressure (bar)**
Step 0: 0	15.01 ± 1.07	10.00
Step 1: 1250	15.68 ± 1.47	10.50
Step 2: 2500	15.81 ± 1.67	10.00
Step 3: 5000	16.12 ± 0.50	10.00
Step 4: 10000	16.02 ± 0.93	10.00
Step 5: 20000	14.72 ± 0.68	10.00

Table 22. Averaged permeate flux data acquired with MATLAB, related standard deviation and measured pressure as salinity increases for replicate 2 of the XPNF membrane.

XPNF - REP 2		
Nominal additional NaCl concentration (mg/L)	**Average flux (LMH)**	**Pressure (bar)**
Step 0: 0	13.85 ± 0.72	10.00
Step 1: 1250	14.60 ± 0.22	10.00
Step 2: 2500	15.40 ± 0.42	10.00
Step 3: 5000	16.53 ± 0.49	10.00
Step 4: 10000	15.76 ± 1.06	10.00
Step 5: 20000	15.64 ± 0.61	10.00

In addition, it is possible to visualize the trend of these parameters during the entire duration of the test through the following graphs.

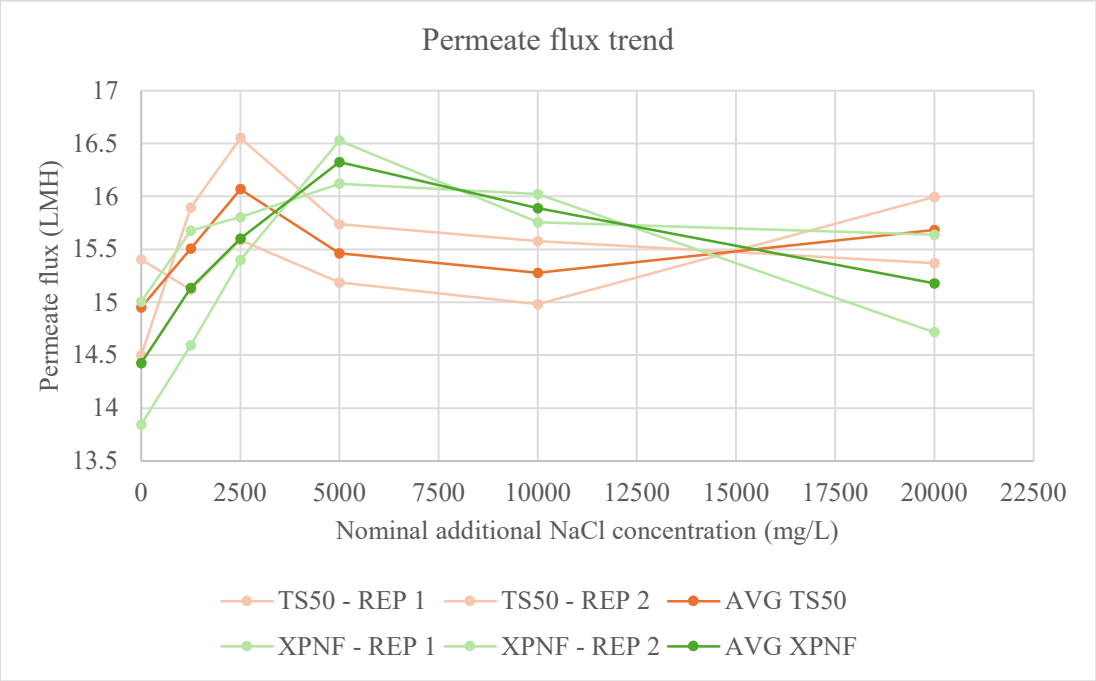


Figure 46. Permeate flux trend as salinity increases, showing both replicates and their average for both membranes.

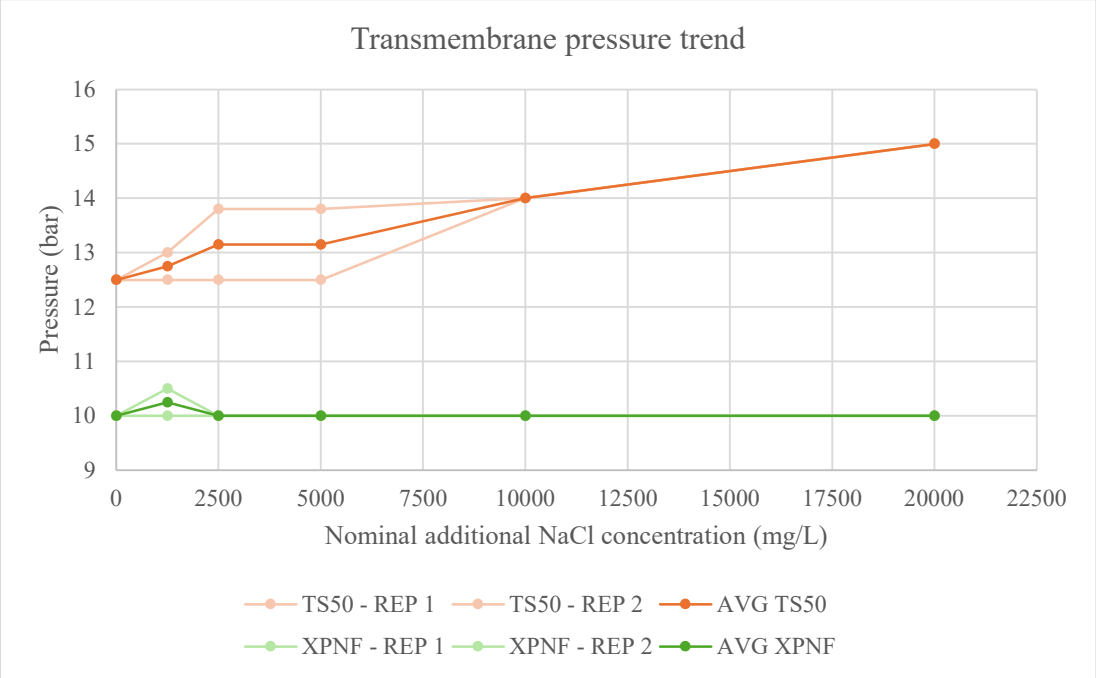


Figure 47. Transmembrane pressure trend as salinity increases, showing both replicates and their average for both membranes.

Subsequently, similarly to Test 2, the concentrations of lithium, magnesium, and sodium ions, as well as the salinity of the feed and permeate solutions, were determined for each experimental step. These data were obtained from chemical analyses performed on samples collected during the tests by an external laboratory.
The results of the chemical analyses are reported in the following tables and form the basis for calculating the main membrane performance parameters.

Table 23. Concentrations of lithium, magnesium and sodium ions and salinity of the feed and permeate solutions as salinity increases for the replicate 1 of the TS50 membrane.

TS50 - REP 1					
	Nominal additional NaCl concentration (mg/L)	**Salinity (mg/L)**	**Li^+ (mg/L)**	**Mg^{2+} (mg/L)**	**Na^+ (mg/L)**
Feed	Step 0: 0	36507	607	5002	2
Feed	Step 1: 1250	39685	563	4666	1343
Feed	Step 2: 2500	42862	694	5849	3322
Feed	Step 3: 5000	49217	624	5190	6049
Feed	Step 4: 10000	61927	484	4052	9495
Feed	Step 5: 20000	87347	450	3752	17846
Permeate	Step 0: 0	5789	665	99	2
Permeate	Step 1: 1250	8648	678	108	1515
Permeate	Step 2: 2500	11508	617	108	2745
Permeate	Step 3: 5000	17227	726	156	6341
Permeate	Step 4: 10000	28666	537	144	9165
Permeate	Step 5: 20000	51544	508	190	17639

Table 24. Concentrations of lithium, magnesium and sodium ions and salinity of the feed and permeate solutions as salinity increases for the replicate 2 of the TS50 membrane.

TS50 - REP 2					
	Nominal additional NaCl concentration (mg/L)	**Salinity (mg/L)**	**Li^+ (mg/L)**	**Mg^{2+} (mg/L)**	**Na^+ (mg/L)**
Feed	Step 0: 0	36507	525	4300	4
Feed	Step 1: 1250	39685	700	5834	1669
Feed	Step 2: 2500	42862	584	4855	2775
Feed	Step 3: 5000	49217	630	5309	6002
Feed	Step 4: 10000	61927	472	3934	9129
Feed	Step 5: 20000	87347	475	3971	18564
Permeate	Step 0: 0	5789	516	70	3
Permeate	Step 1: 1250	8648	562	76	1219
Permeate	Step 2: 2500	11508	626	92	2792
Permeate	Step 3: 5000	17227	607	105	5277
Permeate	Step 4: 10000	28666	532	118	9275
Permeate	Step 5: 20000	51544	507	173	17991

Table 25. Concentrations of lithium, magnesium and sodium ions and salinity of the feed and permeate solutions as salinity increases for the replicate 1 of the XPNF membrane.

XPNF - REP 1					
	Nominal additional NaCl concentration (mg/L)	**Salinity (mg/L)**	**Li^+ (mg/L)**	**Mg^{2+} (mg/L)**	**Na^+ (mg/L)**
Feed	Step 0: 0	36507	554	4546	4
Feed	Step 1: 1250	39685	651	5404	1542
Feed	Step 2: 2500	42862	649	5359	3117
Feed	Step 3: 5000	49217	577	4842	5553
Feed	Step 4: 10000	61927	461	3791	8967
Feed	Step 5: 20000	87347	461	3805	18171
Permeate	Step 0: 0	5789	542	425	4
Permeate	Step 1: 1250	8648	712	615	1623
Permeate	Step 2: 2500	11508	661	633	2950
Permeate	Step 3: 5000	17227	644	780	5582
Permeate	Step 4: 10000	28666	534	858	9442
Permeate	Step 5: 20000	51544	502	1077	14883

Table 26. Concentrations of lithium, magnesium and sodium ions and salinity of the feed and permeate solutions as salinity increases for the replicate 2 of the XPNF membrane.

XPNF - REP 2					
	Nominal additional NaCl concentration (mg/L)	**Salinity (mg/L)**	**Li^+ (mg/L)**	**Mg^{2+} (mg/L)**	**Na^+ (mg/L)**
Feed	Step 0: 0	36507	534	4345	10
Feed	Step 1: 1250	39685	629	5164	1504
Feed	Step 2: 2500	42862	613	5064	2932
Feed	Step 3: 5000	49217	556	4655	5355
Feed	Step 4: 10000	61927	476	3947	9242
Feed	Step 5: 20000	87347	465	3825	18210
Permeate	Step 0: 0	5789	630	514	59
Permeate	Step 1: 1250	8648	721	483	1442
Permeate	Step 2: 2500	11508	855	897	7704
Permeate	Step 3: 5000	17227	675	529	2602
Permeate	Step 4: 10000	28666	540	768	9201
Permeate	Step 5: 20000	51544	515	1097	17831

For Test 3 as well, based on the data obtained from the chemical analyses, the main parameters used to evaluate membrane performance were calculated. Specifically, the actual ionic strength, the observed lithium rejection, the observed magnesium rejection, and the Li/Mg separation factor were determined as in the second test. But since sodium chloride was added in this test to vary the salinity of the solution, the following parameters were also calculated:

- Sodium observed rejection rate

$$R_{Na} = 1 - \frac{C_{Na\ permeate}}{C_{Na\ feed}}$$

- Li, Na separation factor

$$S_{Li,Na} = \frac{\frac{C_{Li\ permeate}}{C_{Li\ feed}}}{\frac{C_{Na\ permeate}}{C_{Na\ feed}}}$$

The values calculated for all parameters are shown in the following tables for both membranes and for each experimental replicate.

Table 27. Calculated values of actual ionic strength (I), lithium rejection rate (R_{Li}), magnesium rejection rate (R_{Mg}), sodium rejection rate (R_{Na}), lithium-magnesium separation factor ($S_{Li, Mg}$) and lithium-sodium separation factor ($S_{Li, Na}$) as salinity increase for the replicate 1 of the TS50 membrane.

TS50 - REP 1						
Nominal additional NaCl concentration (mg/L)	**I (mM)**	**R_{Li} (%)**	**R_{Mg} (%)**	**R_{Na} (%)**	**$S_{Li, Mg}$**	**$S_{Li, Na}$**
Step 0: 0	704.78	-9.65	98.02	0.00	55.35	1.19
Step 1: 1250	715.30	-20.45	97.69	-12.80	52.11	1.07
Step 2: 2500	966.25	11.03	98.16	17.37	48.37	1.08
Step 3: 5000	993.52	-16.28	96.99	-4.82	38.59	1.11
Step 4: 10000	982.76	-10.90	96.45	3.48	31.21	1.15
Step 5: 20000	1304.08	-13.02	94.94	1.16	22.35	1.14

Table 28. Calculated values of actual ionic strength (I), lithium rejection rate (R_{Li}), magnesium rejection rate (R_{Mg}), sodium rejection rate (R_{Na}), lithium-magnesium separation factor ($S_{Li, Mg}$) and lithium-sodium separation factor ($S_{Li, Na}$) as salinity increase for the replicate 2 of the TS50 membrane.

TS50 - REP 2						
Nominal additional NaCl concentration (mg/L)	**I (mM)**	**R_{Li} (%)**	**R_{Mg} (%)**	**R_{Na} (%)**	**$S_{Li, Mg}$**	**$S_{Li, Na}$**
Step 0: 0	606.51	1.77	98.38	0.00	60.10	1.33
Step 1: 1250	893.44	19.73	98.69	26.97	61.21	1.10
Step 2: 2500	803.98	-7.29	98.10	-0.63	56.47	1.07
Step 3: 5000	1006.93	3.58	98.03	12.08	48.89	1.10
Step 4: 10000	950.56	-12.79	96.99	-1.60	37.46	1.11
Step 5: 20000	1365.90	-6.88	95.65	3.09	24.58	1.10

Table 29. Calculated values of actual ionic strength (I), lithium rejection rate (R_{Li}), magnesium rejection rate (R_{Mg}), sodium rejection rate (R_{Na}), lithium-magnesium separation factor ($S_{Li, Mg}$) and lithium-sodium separation factor ($S_{Li, Na}$) as salinity increase for the replicate 1 of the XPNF membrane.

XPNF - REP 1						
Nominal additional NaCl concentration (mg/L)	**I (mM)**	**R_{Li} (%)**	**R_{Mg} (%)**	**R_{Na} (%)**	**$S_{Li, Mg}$**	**$S_{Li, Na}$**
Step 0: 0	641.02	2.16	90.65	0.00	10.47	0.98
Step 1: 1250	827.80	-9.33	88.62	-5.22	9.61	1.04
Step 2: 2500	890.44	-1.79	88.18	5.35	8.61	1.08
Step 3: 5000	922.22	-11.55	83.88	-0.51	6.92	1.11
Step 4: 10000	924.23	-15.78	77.36	-5.29	5.12	1.10
Step 5: 20000	1326.45	-8.89	71.71	18.09	3.85	1.33

Table 30. Calculated values of actual ionic strength (I), lithium rejection rate (R_{Li}), magnesium rejection rate (R_{Mg}), sodium rejection rate (R_{Na}), lithium-magnesium separation factor ($S_{Li, Mg}$) and lithium-sodium separation factor ($S_{Li, Na}$) as salinity increase for the replicate 2 of the XPNF membrane.

XPNF - REP 2						
Nominal additional NaCl concentration (mg/L)	**I (mM)**	**R_{Li} (%)**	**R_{Mg} (%)**	**R_{Na} (%)**	**$S_{Li, Mg}$**	**$S_{Li, Na}$**
Step 0: 0	613.71	-17.87	88.16	0.00	9.96	0.20
Step 1: 1250	793.43	-14.64	90.65	4.13	12.26	1.20
Step 2: 2500	840.82	-39.42	82.29	-162.73	7.87	0.53
Step 3: 5000	887.54	-21.26	88.64	51.41	10.67	2.50
Step 4: 10000	957.64	-13.53	80.54	0.44	5.83	1.14
Step 5: 20000	1331.09	-10.83	71.31	2.08	3.86	1.13

Again, for each calculated parameter, the results obtained in the two experimental replicates were subsequently averaged and their standard deviations determined, to obtain representative and statistically reliable values for membrane performance.
The average values and corresponding standard deviations are shown in the following tables.

Table 31. Average permeate flux, pressure, actual ionic strength (I), lithium rejection rate (R_{Li}), magnesium rejection rate (R_{Mg}), sodium rejection rate (R_{Na}), lithium-magnesium separation factor ($S_{Li, Mg}$) and lithium-sodium separation factor ($S_{Li, Na}$) as salinity increase of the two replicates for the TS50 membrane and the associated standard deviations.

TS50								
Nominal additional NaCl concentration (mg/L)	**Permeate flux (LMH)**	**Pressure (bar)**	**I (mM)**	**R_{Li} (%)**	**R_{Mg} (%)**	**R_{Na} (%)**	**$S_{Li, Mg}$**	**$S_{Li, Na}$**
Step 0: 0	14.95 ± 0.64	12.50 ± 0.00	655.65 ± 69.49	-3.94 ± 8.08	98.19 ± 0.25	-	57.73 ± 3.36	1.26 ± 0.10
Step 1: 1250	15.51 ± 0.55	12.75 ± 0.35	804.37 ± 125.97	-0.36 ± 28.41	98.19 ± 0.71	7.08 ± 28.12	56.66 ± 6.44	1.08 ± 0.02
Step 2: 2500	16.07 ± 0.68	13.15 ± 0.92	885.11 ± 114.74	1.87 ± 12.95	98.13 ± 0.04	8.37 ± 12.73	52.42 ± 5.73	1.07 ± 0.01
Step 3: 5000	15.46 ± 0.39	13.15 ± 0.92	1000.22 ± 9.48	-6.35 ± 14.04	97.51 ± 0.74	3.63 ± 11.95	43.74 ± 7.29	1.10 ± 0.01
Step 4: 10000	15.28 ± 0.42	14.00 ± 0.00	966.66 ± 22.77	-11.84 ± 1.34	96.72 ± 0.38	0.94 ± 3.58	34.33 ± 4.42	1.13 ± 0.03
Step 5: 20000	15.68 ± 0.44	15.00 ± 0.00	1334.99 ± 43.72	-9.95 ± 4.34	95.30 ± 0.50	2.12 ± 1.36	23.46 ± 1.58	1.12 ± 0.03

Table 32. Average permeate flux, pressure, actual ionic strength (I), lithium rejection rate (R_{Li}), magnesium rejection rate (R_{Mg}), sodium rejection rate (R_{Na}), lithium-magnesium separation factor ($S_{Li, Mg}$) and lithium-sodium separation factor ($S_{Li, Na}$) as salinity increase of the two replicates for the XPNF membrane and the associated standard deviations.

XPNF								
Nominal additional NaCl concentration (mg/L)	**Permeate flux (LMH)**	**Pressure (bar)**	**I (mM)**	**R_{Li} (%)**	**R_{Mg} (%)**	**R_{Na} (%)**	**$S_{Li, Mg}$**	**$S_{Li, Na}$**
Step 0: 0	14.43 ± 0.82	10.00 ± 0.00	627.36 ± 19.31	-7.86 ± 14.16	89.41 ± 1.76	-	10.21 ± 0.36	0.59 ± 0.55
Step 1: 1250	15.14 ± 0.77	10.25 ± 0.35	810.61 ± 24.30	-11.98 ± 3.76	98.64 ± 1.43	-0.55 ± 6.61	10.93 ± 1.87	1.12 ± 0.11
Step 2: 2500	15.60 ± 0.29	10.00 ±	865.63 ± 35.08	-20.61 ± 26.61	85.24 ± 4.16	-78.69 ± 118.85	8.24 ± 0.52	0.80 ± 0.39
Step 3: 5000	16.33 ± 0.29	10.00 ± 0.00	904.88 ± 24.52	-16.41 ± 6.87	86.26 ± 3.36	25.45 ± 36.71	8.80 ± 2.65	1.80 ± 0.98
Step 4: 10000	15.89 ± 0.19	10.00 ± 0.00	940.93 ± 23.62	-14.67 ± 1.60	78.95 ± 2.25	-2.42 ± 4.05	5.47 ± 0.51	1.12 ± 0.03
Step 5: 20000	15.18 ± 0.65	10.00 ± 0.00	1328.77 ± 3.28	-9.86 ± 1.37	71.51 ± 0.28	10.09 ± 11.32	3.86 ± 0.01	1.23 ± 0.14

6.3.2 Results interpretation

Actual ionic strength

The addition of NaCl resulted in a progressive increase in the actual ionic strength of the solution, allowing to evaluate the influence of salinity on the ion transport mechanisms through nanofiltration membranes.

Although the nominal NaCl concentration represents the amount of salt added to the solution, it does not fully describe the actual system conditions, since the simultaneous presence of all ions in solution determines an intensity of electrostatic interactions that may differ from that theoretically expected. For this reason, the actual ionic strength was calculated, which represents the true intensity of the ionic field and is a more representative parameter of the operating conditions.

Ionic strength directly influences the electrostatic interactions between ions in solution and the membrane surface. Therefore, it is not the addition of NaCl that directly affects membrane performance, but rather the increase in ionic strength that it induces.

As shown in the graph below, the actual ionic strength progressively increases with increasing NaCl concentration for both membranes. Furthermore, the trend is nearly linear and very similar for both membranes, indicating that the tests were conducted under comparable chemical conditions. The ionic strength therefore represents the reference parameter for interpreting the observed changes in ion rejection and the Li/Mg separation factor with varying salinity.

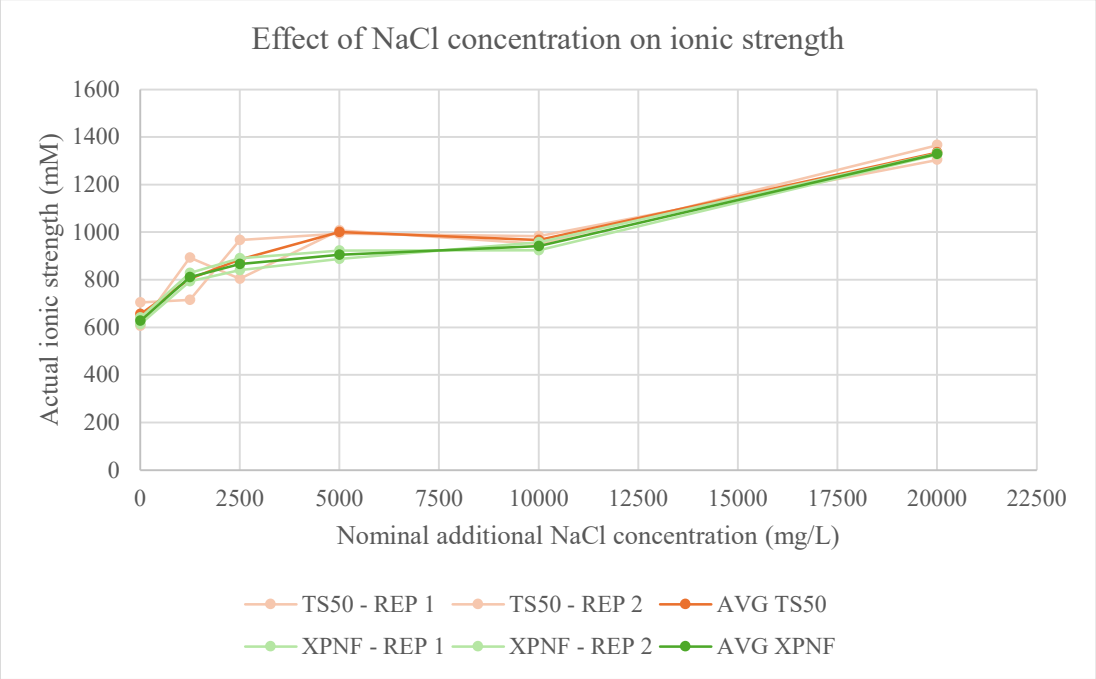


Figure 48. Ionic strength trend as salinity increases, showing both replicates and their average for both membranes.

Lithium rejection

In the Li/Mg separation process, the goal is to promote the passage of lithium ions through the membrane. Therefore, a lithium rejection close to zero represents the ideal behaviour, as it indicates that Li^+ permeates easily and can be recovered in the permeate.

From the analysis of the results, it is observed that, for both membranes, lithium rejection generally remains very low across the entire NaCl concentration range investigated. Although there are fluctuations between the different experimental measurements and between the two replicates, no tendency for rejection to increase or decrease with increasing ionic strength emerges.

These results indicate that Li^+ ion transport through membranes is barely affected by increasing salinity and that lithium continues to permeate effectively even in the presence of high NaCl concentrations. From an application point of view, this behaviour is particularly favourable, as it allows for maintaining high lithium recovery in the permeate even under conditions that simulate those typical of natural brines.

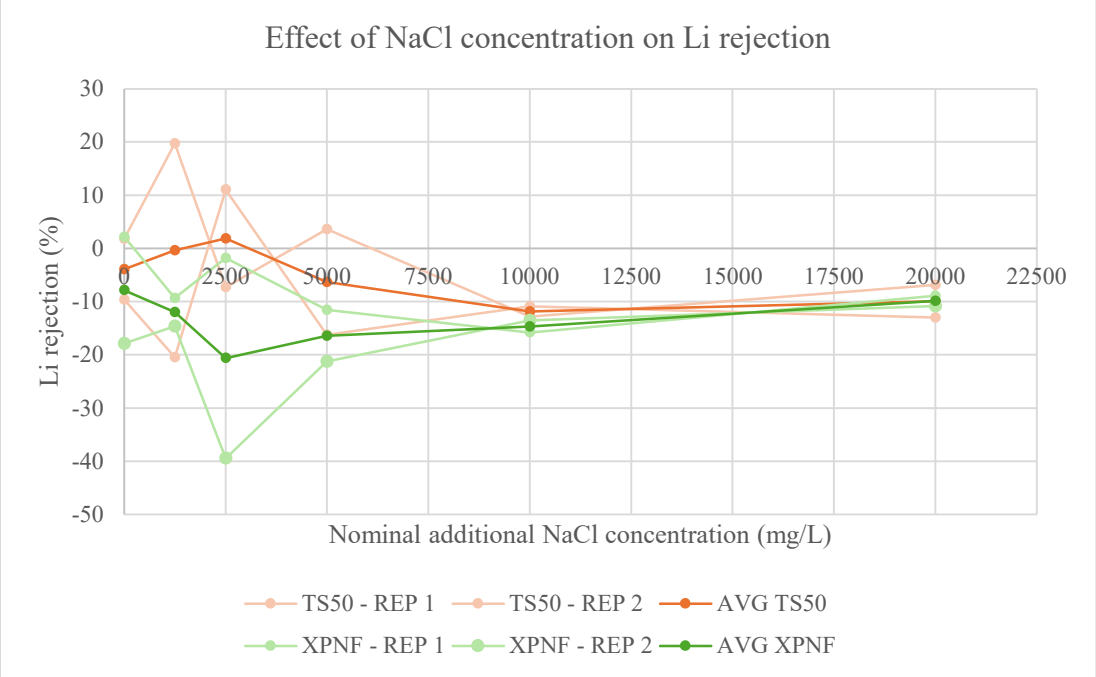


Figure 49. Lithium rejection trend as salinity increases, showing both replicates and their average for both membranes.

Magnesium rejection

Magnesium rejection is a key parameter for evaluating membrane performance, as it describes their ability to retain the main "contaminant" present in the solution. A high Mg^{2+} rejection is essential for limiting permeate contamination and improving the purity of the recovered lithium.

Analysis of the results shows a progressive decrease in Mg^{2+} rejection as the NaCl concentration increases for both membranes. This behaviour is consistent with the increase in the ionic strength of the solution, which further screens the already limited surface charge of the membrane, thereby reducing the residual contribution of Donnan exclusion while also weakening dielectric exclusion, ultimately favouring the passage of magnesium through the membrane.

The reduction in rejection is more marked for the XPNF membrane, while the TS50 membrane maintains higher values across the entire salinity range investigated. This highlights the TS50 membrane's greater ability to maintain its selectivity towards Mg^{2+} even under conditions of high ionic strength, making it more effective at retaining magnesium and reducing permeate contamination.

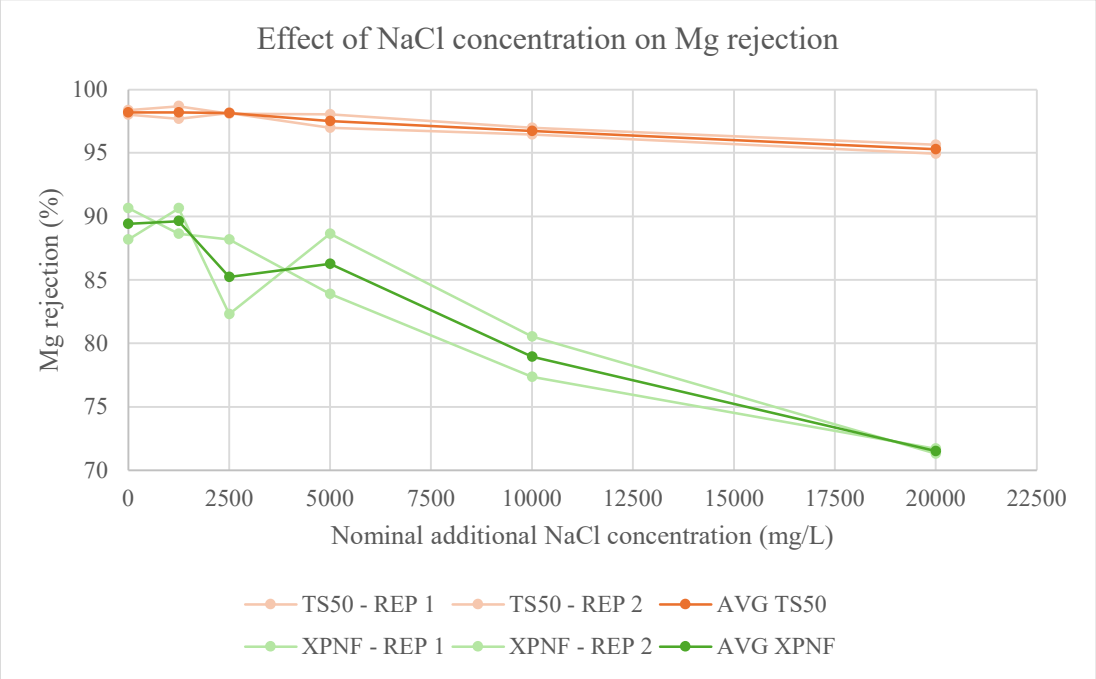


Figure 50. Magnesium rejection trend as salinity increases, showing both replicates and their average for both membranes.

Sodium rejection

Sodium rejection was analysed to compare the behaviour of two monovalent cations, Li^+ and Na^+, with that of the divalent cation Mg^{2+}, allowing an assessment of the influence of ionic valence on the separation mechanisms of nanofiltration membranes. The results show that, despite the fluctuations in the values obtained, the rejection of Na^+ is generally lower than that of Mg^{2+} and exhibits small variations as the NaCl concentration increases. This behaviour is consistent with the monovalent nature of the sodium ion, which is less affected by electrostatic interaction phenomena than divalent ions. In fact, an increase in the ionic strength of the solution reduces the Donnan effect and the dielectric exclusion, but the impact on a monovalent ion is less pronounced than that observed for Mg^{2+}.

The comparison between Li^+, Na^+, and Mg^{2+} shows that ionic valence is one of the main factors regulating transport across nanofiltration membranes.

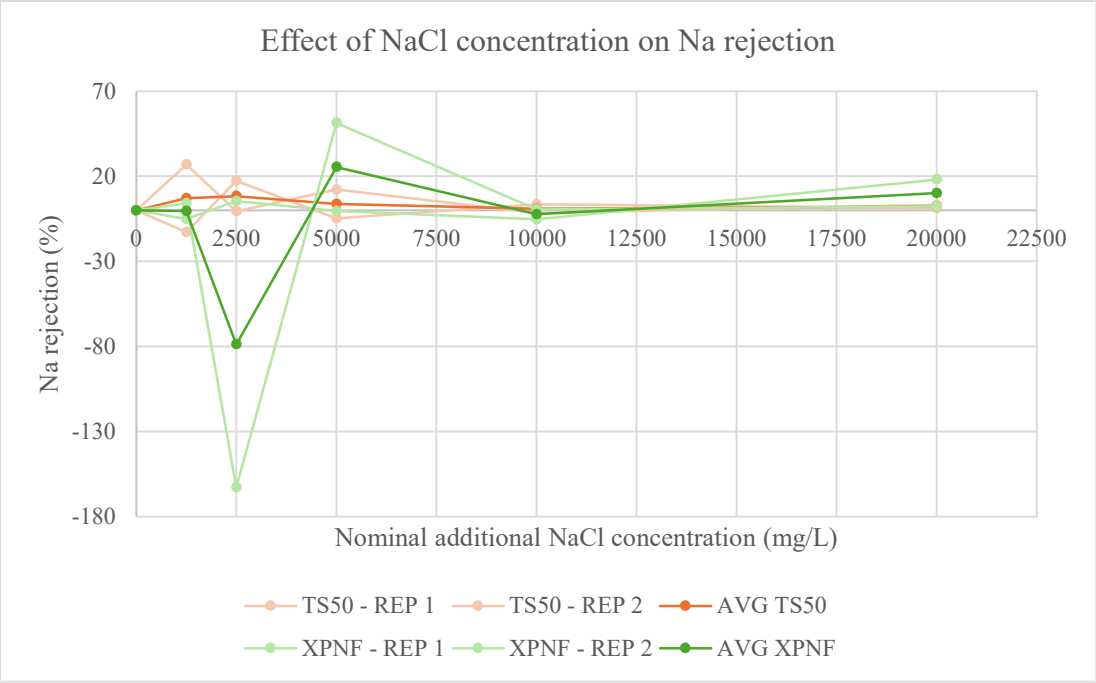


Figure 51. Sodium rejection trend as salinity increases, showing both replicates and their average for both membranes.

Lithium-magnesium separation factor

The Li/Mg separation factor is the most significant parameter for evaluating membrane performance, as it simultaneously describes the membrane's ability to promote the passage of lithium ions and retain magnesium ions. Unlike the rejection of individual ions, this parameter provides an overall measure of the efficiency of the Li^+ and Mg^{2+} separation process: the higher its value, the greater the membrane's ability to selectively recover lithium while minimizing the passage of magnesium into the permeate.

From the analysis of the results, a gradual decrease in the separation factor is observed as the NaCl concentration increases for both membranes. This trend is not attributable to a reduction in lithium permeation, which, as seen before, remains essentially constant throughout the entire salinity range investigated, but rather to the gradual decrease in magnesium rejection. In fact, the increase in the ionic strength of the solution attenuates the Donnan effect and the dielectric exclusion promoting the passage of Mg^{2+} ions through the membrane and resulting in a reduction in overall separation efficiency.

A comparison of the two membranes also shows that the TS50 maintains higher separation factor values than the XPNF under all experimental conditions considered. This indicates that the TS50 is more capable to preserve Li/Mg selectivity even in the presence of high salt concentrations, confirming it as the most promising membrane for selective lithium recovery from high-salinity solutions.

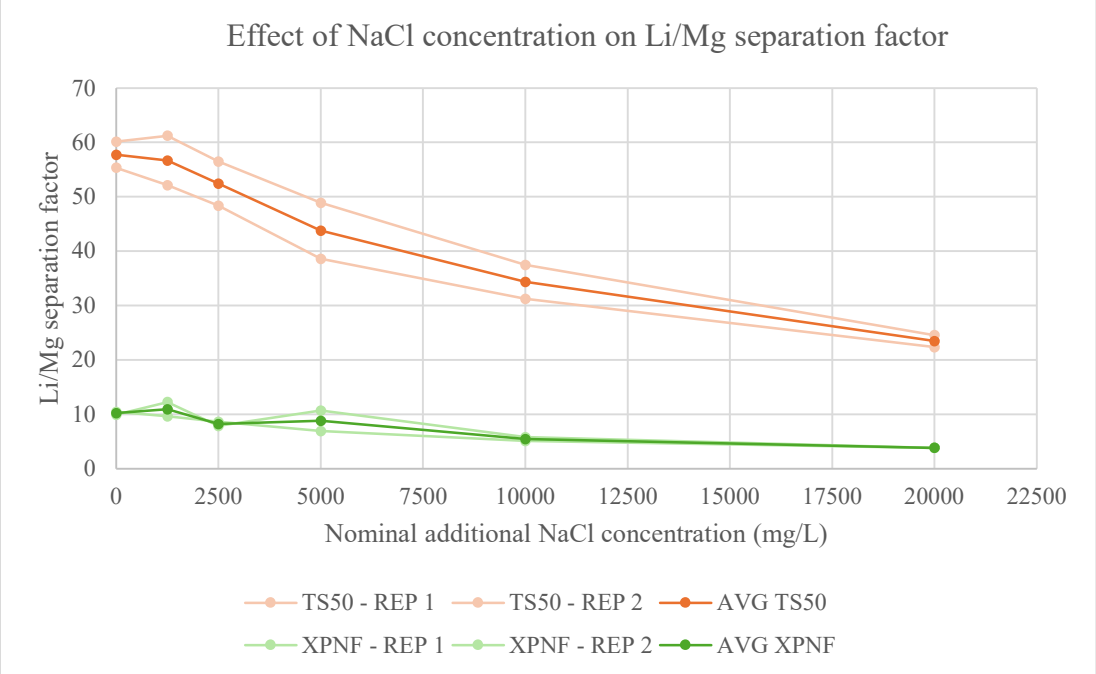


Figure 52. Lithium-magnesium separation factor trend as salinity increases, showing both replicates and their average for both membranes.

Lithium-sodium separation factor

The Li/Na separation factor was finally evaluated to analyse the membrane's ability to discriminate between two monovalent cations, Li^+ and Na^+. Although the primary objective of the process is the selective separation of lithium and magnesium, studying the behaviour of sodium is of particular interest, since it is generally present in natural brines at much higher concentrations than lithium. Consequently, high Na^+ permeation can affect the composition of the permeate and complicate subsequent lithium purification steps.

From the analysis of the results, it can be seen that the Li/Na separation factor remains close to unity across the entire range of NaCl concentrations investigated for both membranes. This indicates a limited ability to discriminate between the two monovalent cations, which have similar chemical and physical properties and interact with the membrane in a similar manner.

Unlike the separation of Li^+ and Mg^{2+}, which is strongly influenced by the ions' different valences and hydration radii, the separation of Li^+ and Na^+ is more difficult. An increase in ionic strength does not significantly alter this behaviour, confirming that the nanofiltration membranes used in this study are unable to effectively separate the two monovalent cations. This result is, however, consistent with what has been reported in the literature.

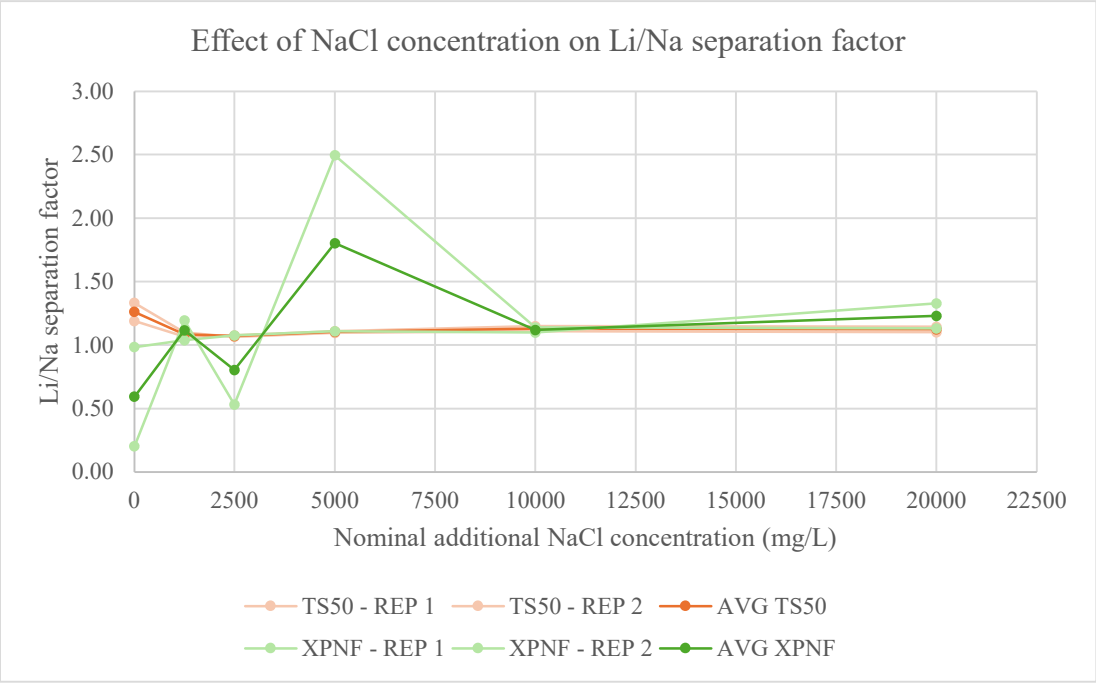


Figure 53. Lithium-sodium separation factor trend as salinity increases, showing both replicates and their average for both membranes.

Overall interpretation

Overall, the results of Test 3 show that salinity is a key operational parameter for the selective separation of Li^+ and Mg^{2+} using nanofiltration membranes. An increase in the NaCl concentration leads to an increase in the ionic strength of the solution, thereby altering the electrostatic interactions that govern ion transport across the membrane.

As explained in Chapter 4, the TS50 and XPNF nanofiltration membranes typically exhibit a negatively charged surface under neutral or alkaline conditions. However, under the acidic conditions employed in this study, the surface charge of the membrane decreases bringing the membrane close to its isoelectric point, causing it to behave as a nearly neutral membrane or even like one with a slight positive charge. Under these conditions, ion transport is governed primarily by steric exclusion and dielectric exclusion, while Donnan exclusion provides only a limited contribution.

In this context, the addition of NaCl significantly increases the ionic strength of the solution and compresses the already small electric double layer surrounding the membrane surface, in fact, the Na^+ and Cl^- ions shield the surface charges of the membrane, causing a rapid attenuation of the electric potential. So, although the membrane surface charge is already substantially reduced under the acidic conditions, the increased ionic strength further screens any residual surface charges, leading to a further weakening of the already limited Donnan exclusion. Consequently, electrostatic interactions contribute only marginally to ion separation. At the same time, the increase in ionic strength also weakens dielectric exclusion, which is important for divalent ions because its contribution is proportional to the square of the ionic valence. Consequently, the electrostatic barrier opposing the transport of Mg^{2+} becomes less effective, leading to the progressive decrease in magnesium rejection observed experimentally. [28]

The transport of Li^+ ions, on the other hand, is much less affected by an increase in ionic strength. As a monovalent cation, lithium is less affected by the electrostatic interactions responsible for the Donnan effect and dielectric exclusion; consequently, its permeation remains essentially constant even in the presence of high concentrations of NaCl, as confirmed by the rejection values close to zero obtained experimentally.

It should be noted that the rejection of Mg^{2+} does not depend exclusively on the electrostatic interactions. Magnesium has a larger hydrated radius and hydration energy than lithium and sodium, characteristics that further hinder its transport across the membrane by steric exclusion. For this reason, although increased salinity and

consequently ionic strength reduce the efficiency of electrostatic and dielectric exclusion, the rejection of Mg^{2+} decreases only partially.

Therefore, when comparing the two membranes, the TS50 consistently maintained higher magnesium rejection values and Li/Mg separation factors than the XPNF in all tests conducted; this behaviour indicates that the TS50 is better able to maintain its selectivity even under conditions of high salinity and so also ionic strength, confirming it, also in this third test, as the most promising membrane for selective lithium recovery from high-salinity brines.

7. Conclusion

In conclusion, the objective of this thesis work was to evaluate the performance of two commercial nanofiltration membranes, TS50 and XPNF, produced by the MANN+HUMMEL company, in the selective separation of lithium and magnesium ions, in order to assess their potential use in Direct Lithium Extraction (DLE) processes from brines.

To achieve this objective, an experimental campaign was conducted consisting of three different types of tests. The first was dedicated to the hydraulic characterization of the membranes, through the determination of intrinsic permeance and theoretical selectivity based on magnesium sulphate rejection. In the second test, lithium–magnesium separation tests were performed under standard operating conditions to evaluate the membrane's selectivity in the presence of a solution containing these two ions. Finally, in the third test, experiments were conducted with increasing concentrations of sodium chloride to assess the influence of salinity on the membranes' performance in lithium–magnesium separation.
The experimental results confirmed that both membranes can promote the passage of lithium ions over magnesium ions, highlighting the potential of these nanofiltration membranes for applications involving the selective recovery of lithium from brines, even under acidic conditions where the membrane surface charge is substantially reduced and so Donnan exclusion is limited. However, a comparison of the two materials revealed significant differences.

Regarding the first test, the TS50 membrane exhibited higher values for both intrinsic permeance and magnesium sulphate rejection (and thus theoretical selectivity) compared to the XPNF. This result is particularly interesting, since nanofiltration membranes generally involve a trade-off between permeance and selectivity: an increase in permeance is often associated with a reduction in solute retention capacity and, consequently, in selectivity. In the case of the TS50, however, both properties are improved compared to the XPNF, indicating a particularly favourable combination of high permeance and selectivity.
In the second test, instead, the XPNF membrane showed a slightly lower lithium rejection rate and, consequently, greater Li^+ permeation. However, the TS50 maintained a significantly higher magnesium rejection rate, resulting in a much higher Li/Mg separation factor. Given that the separation factor is the most representative parameter of the process's overall efficiency, the TS50 also demonstrated better performance in this phase.

Finally, the third test showed that an increase in the concentration of sodium chloride in the feed solution affects the behaviour of the membranes. The main effects of these changes in behaviour were an increase in ionic strength and a subsequent decrease in magnesium rejection and in the lithium-magnesium separation factor. However, despite this decrease in performance, the TS50 membrane maintained higher magnesium rejection and separation factor values than the XPNF, demonstrating a greater ability to maintain selectivity even under conditions of high salinity.

Overall, the results obtained identify TS50 as the most promising membrane among those analysed for selective lithium recovery from brines. The balance between permeance, high magnesium rejection, and good lithium permeability makes it particularly interesting for potential use in Direct Lithium Extraction processes.

7.1 Future developments

The experimental work carried out in this thesis represents a screening phase for the membranes under investigation. Future developments in this work will focus on evaluating their performance under operating conditions that more closely resemble those of an actual industrial lithium direct extraction process.

Specifically, the membranes will undergo high-recovery separation tests. Unlike the tests carried out in this study, which were conducted with zero recovery and thus with a basically constant solution composition, these tests involve a high percentage of permeate recovery. Consequently, during the experiment, the feed solution becomes progressively more concentrated, leading to an increase in ionic strength and progressively more severe separation conditions.

These tests will make it possible to evaluate the membrane's behaviour under conditions that more closely resemble those of actual industrial applications, verifying the stability of the permeate flow, lithium–magnesium selectivity, and overall performance as the solution concentration increases, thereby confirming the membrane's effective reliability under the operating conditions required by Direct Lithium Extraction processes.

References

[1] L. V. Garcia, Y.-C. Ho, M. M. Myo Thant, D. S. Han, and J. W. Lim, 'Lithium in a Sustainable Circular Economy: A Comprehensive Review', *Processes*, vol. 11, no. 2, p. 418, Jan. 2023, doi: 10.3390/pr11020418.

[2] H. M. Akbar *et al.*, 'Lithium Extraction Methodology and Recovery from Conventional Resources: A Critical Review', *Water Air Soil Pollut*, vol. 236, no. 11, p. 723, Nov. 2025, doi: 10.1007/s11270-025-08382-4.

[3] C. Trento, 'Lithium element properties and uses', Stanford advanced materials. [Online]. Available: https://www.samaterials.it/blog/lithium-element-properties-and-uses.html

[4] F. Wu, K. R. Shivakumar, K. O. Konhauser, and D. S. Alessi, 'Lithium resources and novel strategies for their extraction and purification', *npj Mater. Sustain.*, vol. 3, no. 1, p. 30, Sep. 2025, doi: 10.1038/s44296-025-00069-5.

[5] N. Mamula, 'Mineral Commodity Summaries 2026', 2026, [Online]. Available: https://pubs.usgs.gov/periodicals/mcs2026/mcs2026.pdf

[6] B. Jaskula, 'Mineral Commodity Summaries 2025', 2025, [Online]. Available: https://pubs.usgs.gov/periodicals/mcs2025/mcs2025-lithium.pdf

[7] B. Jaskula, 'Mineral Commodity Summaries 2024', 2024, [Online]. Available: https://pubs.usgs.gov/periodicals/mcs2024/mcs2024-lithium.pdf

[8] B. Jaskula, 'Mineral Commodity Summaries 2023', 2023, [Online]. Available: https://pubs.usgs.gov/periodicals/mcs2023/mcs2023-lithium.pdf

[9] B. Jaskula, 'Mineral Commodity Summaries 2022', 2022, [Online]. Available: https://pubs.usgs.gov/periodicals/mcs2022/mcs2022-lithium.pdf

[10] B. Jaskula, 'Mineral Commodity Summaries 2021', 2021, [Online]. Available: https://pubs.usgs.gov/periodicals/mcs2021/mcs2021-lithium.pdf

[11] B. Jaskula, 'Mineral Commodity Summaries 2020', 2020, [Online]. Available: https://pubs.usgs.gov/periodicals/mcs2020/mcs2020-lithium.pdf

[12] B. Jaskula, 'Mineral Commodity Summaries 2019', 2019, [Online]. Available: https://d9-wret.s3-us-west-2.amazonaws.com/assets/palladium/production/atoms/files/mcs-2019-lithi.pdf

[13] B. Jaskula, 'Mineral Commodity Summaries 2018', 2018, [Online]. Available: https://d9-wret.s3-us-west-2.amazonaws.com/assets/palladium/production/mineral-pubs/lithium/mcs-2018-lithi.pdf

[14] B. Jaskula, ‘Mineral Commodity Summaries 2017’, 2017, [Online]. Available: https://d9-wret.s3-us-west-2.amazonaws.com/assets/palladium/production/mineral-pubs/lithium/mcs-2017-lithi.pdf

[15] B. Jaskula, ‘Mineral Commodity Summaries 2016’, 2016, [Online]. Available: https://d9-wret.s3-us-west-2.amazonaws.com/assets/palladium/production/mineral-pubs/lithium/mcs-2016-lithi.pdf

[16] H. Strathmann, ‘Membrane Separation Processes, 1. Principles’, in *Ullmann’s Encyclopedia of Industrial Chemistry*, 1st edn, Wiley-VCH, Ed., Wiley, 2011. doi: 10.1002/14356007.a16_187.pub3.

[17] N. Abdullah, M. A. Rahman, M. H. Dzarfan Othman, J. Jaafar, and A. F. Ismail, ‘Membranes and Membrane Processes’, in *Current Trends and Future Developments on (Bio-) Membranes*, Elsevier, 2018, pp. 45–70. doi: 10.1016/B978-0-12-813549-5.00002-5.

[18] R. W. Baker, *Membrane technology and applications*. in McGraw-Hill professional engineering. New York: McGraw-Hill, 2000.

[19] H. Strathmann, ‘Membrane Separation Processes, 2. Design and Operation’, in *Ullmann’s Encyclopedia of Industrial Chemistry*, Wiley-VCH Verlag GmbH & Co. KGaA, Ed., Weinheim, Germany: Wiley-VCH Verlag GmbH & Co. KGaA, 2011, p. o16_o03. doi: 10.1002/14356007.o16_o03.

[20] A. Tiraferri, ‘Membrane-based water and wastewater treatment’, presented at the Applied environmental engineering, 2024 2023.

[21] MANN+HUMMEL, ‘Membrane Chemistry Cellulose Acetate vs. Thin-Film Composite’. Jul. 01, 2021.

[22] L. Zhang, M. Hu, B. He, H. Pei, X. Li, and H. Matsuyama, ‘A review of the nanofiltration membrane for magnesium and lithium separation from salt-lake brine’, *Separation and Purification Technology*, vol. 354, p. 129169, Feb. 2025, doi: 10.1016/j.seppur.2024.129169.

[23] H. Wen, Z. Liu, J. Xu, and J. P. Chen, ‘Nanofiltration membrane for enhancement in lithium recovery from salt-lake brine: A review’, *Desalination*, vol. 591, p. 117967, Dec. 2024, doi: 10.1016/j.desal.2024.117967.

[24] S. Das, E. Deng, A. M. Tandel, S. Singh, J. V. Mowatt, and H. Lin, ‘Nanofiltration Membranes for Li^+/Mg^{2+} Separation: Materials and Mechanisms’, *Journal of Polymer Science*, vol. 64, no. 1, pp. 129–162, Jan. 2026, doi: 10.1002/pol.20250715.

[25] W. Li, J. Tian, Y. Zhao, J. He, L. Pei, and H. Liu, 'Nanofiltration Membranes for High-Selectivity Separation of Li^+ and Mg^{2+} From Salt Lake Brines: Strategies, Challenges, and Perspectives', *Rare Metals*, vol. 45, no. 3, p. e70156, Mar. 2026, doi: 10.1002/rar2.70156.

[26] Y. Zhao, N. Mamrol, Y. Qiu, and B. Van Der Bruggen, 'Introduction to Functional Membranes', in *Advances in Functional Separation Membranes*, X. Li, J. Lin, and S. Zhao, Eds, The Royal Society of Chemistry, 2021, pp. 1–27. doi: 10.1039/9781839165436-00001.

[27] Y. Li, Y. Zhao, H. Wang, and M. Wang, 'The application of nanofiltration membrane for recovering lithium from salt lake brine', *Desalination*, vol. 468, p. 114081, Oct. 2019, doi: 10.1016/j.desal.2019.114081.

[28] Y. Li, Y. Zhao, and M. Wang, 'Effects of pH and salinity on the separation of magnesium and lithium from brine by nanofiltration', *Desalination and Water Treatment*, vol. 97, pp. 141–150, Nov. 2017, doi: 10.5004/dwt.2017.21606.

[29] T. Zhang, W. Zheng, Q. Wang, Z. Wu, and Z. Wang, 'Designed strategies of nanofiltration technology for Mg2+/Li+ separation from salt-lake brine: A comprehensive review', *Desalination*, vol. 546, p. 116205, Jan. 2023, doi: 10.1016/j.desal.2022.116205.

[30] Y. Sun, Q. Wang, Y. Wang, R. Yun, and X. Xiang, 'Recent advances in magnesium/lithium separation and lithium extraction technologies from salt lake brine', *Separation and Purification Technology*, vol. 256, p. 117807, Feb. 2021, doi: 10.1016/j.seppur.2020.117807.

[31] X. Li, Y. Mo, W. Qing, S. Shao, C. Y. Tang, and J. Li, 'Membrane-based technologies for lithium recovery from water lithium resources: A review', *Journal of Membrane Science*, vol. 591, p. 117317, Dec. 2019, doi: 10.1016/j.memsci.2019.117317.